DEVELOPMENT OF THE OVERLAY FORMULATION IN FINITE ELEMENT MODEL

RDU170383

15/05/2017 - 14/11/2019

Lists of Researcher

1	01146	MOHD AKRAMIN BIN MOHD ROMLAY	Ketua
2	0298	MOHD ZAIDI BIN SIDEK	Ahli
3	1965	AHMED NURYE OUMER	Ahli
4	0519	AMIRRUDDIN BIN ABDUL KADIR	Ahli
5	01068	WAN ANUAR BIN WAN HASSAN	Ahli
6	0732	MAHDHIR BIN MOHD YUSOF	Ahli

Halaman dedikasi/penghargaan

Alhamdulillah, first and foremost, I thanks Allah S.W.T. for endowing me with ‘taufiq’, patience and knowledge to complete this research work. My deep gratitude and appreciation goes to my research members, for their extensive guidance, support and enthusiasm in all phases of this work. My appreciation also dedicated to all technical and admin staffs who helped me to smoothen the progress of this research.

Abstract

Fatigue failure is expected to contribute to injuries and financial losses in industries. The complex interaction between the load, time and environment is a major factor that leads to failure. In addition, the material selection, geometry, processing and residual stresses produce uncertainties and possible failure modes in the field of engineering. The conventional approach is to allow the safety factor approach to deal with the variations and circumstances as they occur within the engineering applications. The problems may persist in the computational analysis, where a complex model, such as a three-dimensional surface crack, may require many degrees of freedom during the analysis. The involvement of uncertainties in variables brings the analysis to a higher level of complexity due to the integration of non-linear functions during a probabilistic analysis. Probabilistic methods are applicable in industries such as the maintenance of aircraft structures, airframes, biomechanical systems, nuclear systems, pipelines and automotive systems. Therefore, a plausible analysis that caters for uncertainties and fatigue conditions is demanded. The main objective of this research work was to develop a model for uncertainties in fatigue analysis. The aim was to identify a probabilistic distribution of crack growth and stress intensity factors for surface crack problems. A sensitivity analysis of all the parameters was carried out to identify the most significant parameters affecting the results. The simulation time and the number of generated samples were presented as a measurement of the sampling efficiency and sampling convergence. A finite thickness plate with surface cracks subjected to random constant amplitude loads was considered for the fracture analysis using a newly developed Probabilistic S-version Finite Element Model (ProbS-FEM). The ProbS-FEM was an expansion of the standard finite element model (FEM). The FEM was updated with a refined mesh (*h*-version) and an increased polynomial order (*p*-version), and the combination of the *h*-*p* version was known as the S-version finite element model. A probabilistic analysis was then embedded in the S-version finite element model, and it was then called the ProbS-FEM. The ProbS-FEM was used to construct a local model at the vicinity of the crack area. The local model was constructed with a denser mesh to focus the calculation of the stress intensity factor (SIF) at the crack front. The SIF was calculated based on the virtual crack closure method. The possibility of the crack growing was based on the comparison between the calculated SIF and the threshold SIF. The fatigue crack growth was calculated based on Paris' law and Richard's criterion. In order to obtain an effective sampling strategy, the Monte Carlo and Latin hypercube sampling were employed in the ProbS-FEM. The specimens with a notch were prepared and subjected to fatigue loading for verification of the ProbS-FEM results. The ProbS-FEM was verified for the SIF calculation, the crack growth for mode I and the mixed mode, and the prediction of fatigue life. The major contribution of this research is to the development of a probabilistic analysis for the S-version finite element model. The formulation of uncertainties in the analysis was presented with the ability to model the distribution of the surface crack growth. The ProbS-FEM was shown to resolve the problem of uncertainties in fatigue analysis. The ProbS-FEM can be further extended for a mixed mode fracture subjected to variable amplitude loadings in an uncertain environment.

Abstrak

Kegagalan lesu telah menyumbang kepada kecederaan dan kerugian dalam industri. Interaksi kompleks antara beban, masa dan persekitaran adalah faktor utama yang membawa kepada kegagalan. Di samping itu, pemilihan bahan, geometri, pemprosesan dan tegasan baki menghasilkan ketidakpastian dan mod kegagalan yang mungkin berlaku dalam bidang kejuruteraan. Pendekatan konvensional menggunakan kaedah faktor keselamatan bagi menangani perubahan dan sebarang kemungkinan yang berlaku semasa applikasi kejuruteraan. Masalah berterusan dalam analisis pengiraan, di mana model yang kompleks seperti permukaan retak tiga-dimensi memerlukan darjah kebebasan yang banyak. Penglibatan unsur ketidakpastian dalam pembolehubah membawa analisis ke tahap yang lebih rumit. Ia disebabkan oleh integrasi fungsi bukan linear semasa analisis kebarangkalian. Kaedah kebarangkalian boleh digunakan didalam industri penyelenggaraan struktur pesawat, sistem biomekanik, sistem senjata nuklear, saluran paip dan automotif. Oleh itu, analisis yang munasabah dengan mengambil kira keadaan ketidaktentuan dan kelesuan diperlukan. Objektif utama penyelidikan ini adalah untuk membangunkan satu model ketidaktentuan bagi analisis kelesuan. Tujuannya ialah untuk mengenal pasti taburan kebarangkalian pertumbuhan retak dan faktor keamatan tegasan. Analisis sensitiviti bagi semua pembolehubah dilakukan bagi mengenal pasti pembolehubah yang paling berpengaruh terhadap kegagalan. Masa simulasi dan jumlah sampel yang dihasilkan dibentangkan sebagai pengukuran kepada kecekapan dan penumpuan persampelan. Satu plat dengan ketebalan terbatas yang mempunyai retak permukaan dan bebanan rawak yang berterusan di analisis menggunakan kaedah kebarangkalian Model Unsur Terhingga Versi-S (ProbS-FEM). ProbS-FEM dikembangkan daripada model unsur terhingga (FEM) yang biasa. FEM telah dikemas kini dengan jaringan halus (versi-*h*) dan peningkatan kuasa polinomial (versi-*p*) dan hasil gabungan versi *h*-*p* dipanggil sebagai model unsur terhingga versi-S. Kemudian, analisis kebarangkalian disertakan di dalam model unsur terhingga versi-S dan diberi nama ProbS-FEM. ProbS-FEM menggunakan kaedah pembinaan model tempatan di sekitar kawasan retak. Model tempatan dibina dengan jejaring yang lebih padat untuk memberi tumpuan terhadap pengiraan faktor keamatan tekanan (SIF) pada bahagian retak hadapan. SIF dikira berdasarkan kaedah penutupan retak maya. Kebarangkalian retak untuk berkembang adalah berdasarkan kepada perbandingan di antara nilai SIF yang dikira dan nilai SIF ambang. Pertumbuhan retak lesu dikira berdasarkan model Paris dan kriteria Richard. Persampelan Monte Carlo dan Latin hiperkiub digunakan di dalam ProbS-FEM untuk mendapatkan srategi persampelan yang berkesan. Spesimen-spesimen dengan takuk disediakan dan diuji dengan bebanan lesu untuk tujuan pengesahan. Probs-FEM disahkan dengan pengiraan SIF; pertumbuhan retak untuk mod I dan mod campuran; dan ramalan hayat lesu. Sumbangan utama kajian ini ialah pembangunan analisis kebarangkalian untuk model unsur terhingga versi-S. Formula ketidaktentuan didalam analisis telah dibentangkan dengan keupayaan untuk memodelkan taburan pertumbuhan permukaan-retak. ProbS-FEM telah menunjukkan keupayaan untuk menyelesaikan masalah ketidaktentuan dalam analisis kelesuan. Ia boleh dikembangkan lagi untuk kes mod patah campuran dengan beban amplitud berubah-ubah dalam persekitaran yang tidak menentu.

Contents

Halaman Senarai Rajah

Halaman Senarai Simbol/Singkatan/Tatanama/Istilah

a	initial crack depth
a/c	aspect ratio
b	length of specimen
B^G	deformation matrix for global
B^L	deformation matrix for local
c	initial crack length
C	Paris coefficient c
C^I	constant of VCCM
D	material properties matrix
da	crack growth increment
da_{max}	maximum crack growth increment
$\frac{da}{dN}$	crack growth rate
E	modulus of elasticity
$E[\ ]$	mean operator
f	body force
F_G	force for global region
F_L	force for local region
F_{max}	maximum stress during loading cycle
F_{min}	minimum stress during loading cycle
G_{Total}	total energy release rate
$G_{I,II,III}$	energy release rate for mode I, II & III
h	width of specimen
I	node number around the crack tip
K	stiffness matrix
K_{IC}	critical stress intensity factor
K_{GG}	stiffness matrix for global region
K_{LL}	stiffness matrix for local region
K_{GL}	stiffness matrix for overlay region
$K_{I,II,III}$	stress intensity factor for mode I, II & III
n	fatigue power parameter
P_i^I	nodal force
P_f	failure probability
r	radius of crack growth
R	radius of crack front
S_1^J	area after crack front
S_2^J	area before crack front

t	thickness of specimen
u	displacement function
u^G	displacement function for global
u^L	displacement function for local
$Var[\ ]$	variance operator
w^J	width of element parallel to the crack front
ν_i^I	nodal displacement between the upper and lower crack surfaces
ν_i	crack opening displacement at the crack surface
ν	Poisson's ratio
Δ	width of the element in the radial direction
ΔK_{th}	threshold value
ΔK_{eq}	equivalent stress intensity factor
$\Delta K_{eq_{max}}$	maximum equivalent stress intensity factor
Ω^L	local mesh region
Ω^G	global mesh region
ε	strain
ε^L	strain for local region
ε^G	strain for global region
θ	surface crack angle
φ_o	crack growth angle
σ	stress
σ_{3i}	cohesive stress at the local axis x_3
Γ	boundary condition
Γ^{GL}	boundary condition at overlay region
μ	shear modulus

Halaman Senarai Lampiran

None

Bab 1

Pengenalan

In Finite Element Model (FEM), the crack shape needs to be reconstructed, in order to simulate the behaviours of 3-dimensional surface crack growth. Since the crack shape frequently change by the fatigue crack growth, it is essential to remodel the mesh at the vicinity of the crack tip. The remodel process is time consuming and deals with a complicated solution especially when the structure is subjected to mixed mode loading. The overlay formulation on the subdomain of finite element mesh was introduced to untie the unnecessary relation between the finite element mesh. The objective of this study is to develop an overlay formulation for surface crack propagation analysis. To achieve the objective, the global-local formulation needs to be modelled for used in crack closure integral. After modelling of the global-local formulation is performed, then the validation with the case study thru experimental work is implemented. With the implementation, it is expected to have new global-local element formulation in numerical simulation and new source code for surface crack propagation analysis to specialise for all finite element software. A few typical structural components with the existence of surface crack such as cracked plate [1, 2], cracked round bar [3-6], cracked pipes [7], cracked shells [8, 9], cracked in notched structural components [10, 11]. Those components lead to a failure in the industrial such as petrochemical, aircraft, aerospace, marine structures and others.

From the engineering point of view, the failure of structure is lead by the combination of three basic fracture modes (Mode I, II and III). However, the interfacial defects and self-interstitials as well give some effect to the propagation of crack and finally, the failure of the structure. Due to interstitials, the forces are not balanced in the same way as for another part in the structure, which results in lattice distortion around the defect. Meanwhile, for the interfacial defects, it introduced unbalanced forces which result in relaxation. Therefore, purely analytical solutions provide an incomplete picture of reality. A model in finite element needs to be developed in order to characterise the material imperfections.

Based on the majority of work published, the efficiency of FEM can be substantially increased if the unnecessary linkage between mesh and region's orientation is untied [12]. The various technique has been applied in order to diagnose the problem such as Finite Element Alternating Method (FEAM)[13] and X-FEM [14]. In the both methods, stress field for the crack tip is calculated from singularity function. Meanwhile, a technique without reconstructing the whole finite element mesh is introduced by [15]. The technique requires the generation of automatic mesh around the crack tip. Then the mesh around the crack tip is overlaid on the whole mesh of complete model. Thus, generation of element formulation for the overlaid region is essential since the calculation of stress intensity factor is based on mesh around the crack tip [16]. In addition, the problem with crack surfaces singularities brought the application of overlay formulation for surface crack analysis into fuzzy since the evaluation of stress intensity factor was not clear.

The main goal of this study is to develop an element formulation for the overlay mesh in FEM for the surface crack problem. The overlay formulation consists of global and local element formulation. By overlay the local on the global mesh, the surface crack propagation can be modelled efficiently without distorted element with the evaluation of stress intensity factor. Finite element model with overlay formulation is expected to have such new global-local element formulation in numerical simulation for surface crack propagation and new source code for more accurate crack propagation analysis.

References

1. Dong, Y., et al., SIF solution for a single hole-edge crack in a finite plate with clamped ends. Yingyong Lixue Xuebao/Chinese Journal of Applied Mechanics, 2015. 32(2): p. 187-191.
2. Peng, C., W. Wu, and B. Zhang, Three-dimensional simulations of tensile cracks in geomaterials by coupling meshless and finite element method. International Journal for Numerical and Analytical Methods in Geomechanics, 2015. 39(2): p. 135-154.
3. Toribio, J., et al., Evolution of crack paths and compliance in round bars under cyclic tension and bending. Theoretical and Applied Fracture Mechanics, 2015(0).
4. Toribio, J., et al., Numerical modelling of cracking path in round bars subjected to cyclic tension and bending. International Journal of Fatigue, 2014. 58(0): p. 20-27.

5. Carpinteri, A. and S. Vantadori, Sickle-shaped surface crack in a notched round bar under cyclic tension and bending. Fatigue and Fracture of Engineering Materials and Structures, 2009. 32(3): p. 223-232.
6. Carpinteri, A. and S. Vantadori, Sickle-shaped cracks in metallic round bars under cyclic eccentric axial loading. International Journal of Fatigue, 2009. 31(4): p. 759-765.
7. Brighenti, R., External longitudinal flaws in pipes under complex loading. Journal of Pressure Vessel Technology, Transactions of the ASME, 2001. 123(1): p. 139-145.
8. Liu, R., et al., Determination of stress intensity factors for a cracked shell under bending with improved shell theories. Journal of Aerospace Engineering, 2006. 19(1): p. 21-28.
9. Carpinteri, A., R. Brighenti, and S. Vantadori, Notched double-curvature shells with cracks under pulsating internal pressure. International Journal of Pressure Vessels and Piping, 2009. 86(7): p. 443-453.
10. Cendõn, D.A., A.R. Torabi, and M. Elices, Fracture assessment of graphite V-notched and U-notched specimens by using the cohesive crack model. Fatigue and Fracture of Engineering Materials and Structures, 2015. 38(5): p. 563-573.
11. Larrosa, N.O., A. Navarro, and V. Chaves, Calculating fatigue limits of notched components of arbitrary size and shape with cracks growing in mode i. International Journal of Fatigue, 2015. 74: p. 142-155.
12. McCaslin, S.E., et al., Closed-form stiffness matrices for higher order tetrahedral finite elements. Advances in Engineering Software, 2012. 44(1): p. 75-79.
13. Mingrong, C., Compact alternating direction implicit method for two-dimensional time fractional diffusion equation. Journal of Computational Physics, 2012. 231(6): p. 2621-2633.
14. Bonfils, N., N. Chevaugeon, and N. Moës, Treating volumetric inequality constraint in a continuum media with a coupled X-FEM/level-set strategy. Computer Methods in Applied Mechanics and Engineering, 2012. 205-208(1): p. 16-28.
15. Fish, J., The s-version of the finite element method. Computers & Structures, 1992. 43(3): p. 539-547.
16. Liu, P.F., et al., Finite element analysis of postbuckling and delamination of composite laminates using virtual crack closure technique. Composite Structures, 2011. 93(6): p. 1549-1560.

Objektif dan Skop Kajian

The objectives of this study are:

i) To develop a global-local formulation for used in Finite Element Model.
ii) To validate the proposed global-local formulation with experimental work.

Bab 2

PROBABILISTIC FATIGUE SURFACE CRACK GROWTH PREDICTION USING S-VERSION FINITE ELEMENT MODEL

M.N.M. Husnain[1], M.R.M. Akramin[1], Z.L. Chuan[2], M.S. Shaari[3] and Akiyuki Takahashi[4]

[1]Faculty of Mechanical & ManufacturingEngineering,
Universiti Malaysia Pahang, 26600 Pekan,
Pahang Darul Makmur, Malaysia.

[2]Faculty of Industrial Sciences & Technology,
Universiti Malaysia Pahang, Lebuhraya Tun Razak, 26300 Gambang, Pahang
Darul Makmur, Malaysia.

[3]Faculty of Engineering Technology,
Universiti Malaysia Pahang, Lebuhraya Tun Razak, 26300 Gambang, Pahang
Darul Makmur, Malaysia.

[4]Faculty of Science and Technology, Department
of Mechanical Engineering, Tokyo University of Sciences, 2641 Yamazaki,
Noda, Chiba 278-8510, Japan.

Corresponding Author's Email: [1]husnainoh94@gmail.com.my

Article History: Received xxxxx; Revised xxxx; Accepted xxxx

ABSTRACT: Crack growth is defined by the local stress field built around the crack tip by considering linear elastic fracture mechanics (LEFM). Failure of the materials occurs once the stress intensity factor (SIF) overtakes the material fracture toughness. At this level, the crack will grow rapidly resulting in unstable crack growth until a complete fracture happens. The SIF calculation of the materials can be conducted by experimental, theoretical and numerical techniques. Prediction of SIF is crucial to ensure safety life from the material failure. The aim of the simulation study is to evaluate the accuracy of SIF prediction using finite element analysis. The bootstrap resampling method is employed in S-version Finite Element Model (S-FEM) to generate the random variables in this simulation analysis. The SIF analysis studies are promoted by Bootstrap S-version Finite Element Model (BootstrapS-FEM). Virtual Crack Closure-integral method (VCCM) is an important concept to compute the energy release rate and SIF. The semi-elliptical crack shape is applied with different crack shape aspect ratio in this simulation analysis. The BootstrapS-FEM produces the prediction of SIFs for tension model. The mean of BootstrapS-FEM is calculated from one hundred samples of the resampling method. The bounds are computed based on the lower and upper bounds of the hundred samples of BootstrapS-FEM. The prediction of SIFs is validated with Newman-Raju solution and deterministic by S-FEM within 95% confidence bounds. All possible values of SIF estimation by BootstrapS-FEM are plotted in a graph. The mean of the BootstrapS-FEM is referred to as points estimation. The Newman-Raju solution and deterministic S-FEM values are within the 95% confidence bounds. Thus, the BootstrapS-FEM is considered valid for the prediction.

KEYWORDS: *Stress Intensity Factor; S-version Finite Element Model; Bootstrap Resampling Method; Random Variables; Bounds*

1.0 INTRODUCTION

Fatigue crack growth occurs in manufacturing industries in automotive, aerospace, building, and engineering applications. The cracks appear because of inherent defects in the material structures or

the damage would happen during the service life of the fundamental materials. The surface cracks may be different in the number of cracks, locations, sizes, boundary conditions and crack number. The fatigue crack growth thresholds are determined by using load and constant maximum SIF by increasing the load ratio. A finite element analysis (FEA) is carried out in order to acquire the SIF for K_I, K_{II} and K_{III}. The fatigue crack growth rate is returned to the threshold behavior of the material. If the crack propagation occurs immediately before it reaches the threshold value, the SIF is not identified [1]. If the threshold value is higher than the SIF for the crack, the crack I assumes no propagating occurring in this case. There are several factors that effect crack propagation rates near the threshold level such as crack size, loading condition, microstructure and the environment [2]. The fatigue crack growth is dependent on the maximum value of SIF. It is noted the last prediction that is derived mathematically is a closed form of expression for the driving force [3]. Thus, the SIF of the materials is essential to be predicted before it reaches a critical limit. The SIF is one of the Fracture Mechanics parameters that should be studied in this analysis.

Fracture mechanics is developed to describe and solve the limitation of brittle materials under several loadings. Fracture mechanics parameters such as SIF are calculated when the stress field builds around the crack tip. When the SIF reaches a critical state which is a characteristics parameter, the cracks would propagate. The cracks propagated depend on the amount of the loading. If the loading applied is higher, the crack failure propagation occurs fast depending on its material properties [4]. Investigation of the cracking criterion tends to be more suitable based on fracture mechanics. Crack resistance curve will approach from fracture mechanics theory that is not accomplished in energy balance format [5]. The LEFM considers the materials to be in linear elastic and isotropic states. Thus, the stress field near the crack tip is calculated using the theory of elasticity. The cracks will grow when the stresses around the crack tip exceed the material fracture toughness.

LEFM is a suitable concept to obtain accurate computation of SIF [6]. The SIF depends on the stress that acts on the cracks as well as the crack length. As a simple situation, the length of crack in an infinite plate reacts with the tensile load. The tensile stress is perpendicular to the crack surface and the SIF will be produced from its situation [7]. The materials in brittle case undergo a mainly elastic deformation except at small stress around the crack tip. The LEFM is applied when the stress occurs at the stress field and the SIF is characterised at the crack tip. This is one factor to get accurate estimation of SIF in the crack growth propagation. The stresses at the crack tip and deformation can change depending on time or cycles [8], [9]. In LEFM, the SIF and the strain energy release rate are needed as the fracture criteria to determine the complication of crack tip at stress field. The energy release rate is computed by using several methods such as J-Integral or Virtual Crack Closure-integral Method (VCCM). In this analysis, VCCM is needed to solve the computation of energy release rate in three-dimensional crack growth analysis.

The VCCM is extensively used for calculating the energy release rate established on results from a continuum two-dimensional and three-dimensional FEA. When using the mixed mode fracture criterion, the analysis is required to supply the mode separation [10]. The SIF is calculated from the energy release rate and it is the virtual crack extension method. The VCCM is computed from the energy release rate based on the differentiation of stiffness matrix at the crack front. The energy release rate is calculated from the change of potential energy assuming the small amount of crack extension [11]. The computation of energy release rate is quite simple when generated in finite element analysis since VCCM requires the nodal displacement and forces. The mechanical components are important to predict the crack growth in the material structures. It is difficult to analyse a three-dimensional crack growth using a simple FEM. The S-version is introduced to solve crack growth problems.

The computational effort becomes tedious when the iterations of crack propagation increase. An extended FEM is used to avoid mesh dependent difficulties in modeling of crack growth problems. The FEM analysis software is complicated to develop just based on theory, implementation aspect, computational experience and engineering issues. It is related with computer hardware and manpower cost to be solved by the engineering community [14], [15]. By using the S-version, the problem is

effected significantly and provides higher impact in engineering development programme. The crack area is modelled by local mesh in S-version Finite Element Model (S-FEM). Local mesh is re-meshed automatically by combining with auto-mesh method [16]. Furthermore, the modelling of crack shape becomes computational easily in three-dimensional analysis [17], [16]. The solving of residual stress problem occurring at the stress concentration field can be determined accurately [18]. Thus, the SIF is evaluated along the crack front in VCCM. Calculation of SIF requires high computational effort due to repeated geometry modeling. Kikuchi et al. developed combination of S-FEM with auto-meshing method to simulate fatigue crack growth [19].

Failure is governed by stresses in the victinity of the crack tip. The failure occurs when the SIF exceeds the material fracture toughness. The prediction of SIF is important to prevent a rapid crack growth occuring without warning. Thus, the prediction of SIF is simulated by using the BootstrapS-FEM. The comparison is carried out with Newman-Raju solution and deterministic S-FEM. Computation of SIFs by VCCM is widely used in finite element analysis.

2.0 METHODOLOGY

This section focuses on describing growth at the crack front in the BootstrapS-FEM. The SIF and energy release rate are used as key parameters to figure out the crack growth in LEFM. The energy release rate is defined by VCCM. This is used to resolve the direction of the crack growth at the crack front [11]. Figure 2.1 shows the opening displacement where $(\mathrm{i} = 1, 2, 3, 4, 5, 6)$ near of the crack front as P_i, where $(\mathrm{i} = 1, 2, 3, 4, 5, 6)$ in the VCCM. The opening displacement, v_i is shown on the five nodes at the edge of the crack front.

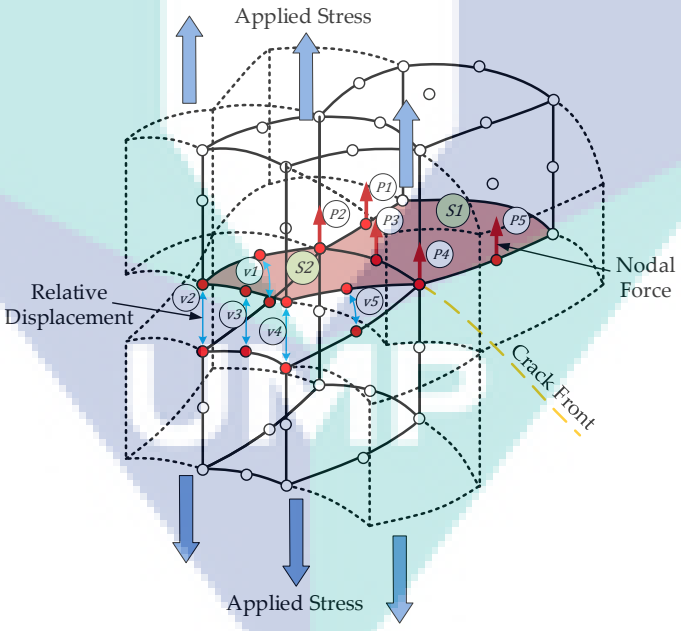

Figure 1: VCCM for local mesh at crack front in three-dimensional analysis

The displacement for the lower surface crack is symbolised by v_{iL} and the displacement of the upper crack surface is symbolised by v_{iU} as shown in Figure 1. Accordingly, the opening displacement, v_i is stated as

$$v_i = v_{iU} - v_{iL} \tag{2.1}$$

The displacement is computed based on summation of global and local displacements for lower and upper surface cracks if the global and local meshes combination are included in the analysis. The calculations of displacement for lower and upper surface cracks are expressed as

$$\begin{aligned} v_{iU} &= v_{iU}^{G} + -v_{iU}^{L} \\ v_{iL} &= v_{iL}^{G} + -v_{iL}^{L} \end{aligned} \tag{2.2}$$

The opening displacement only appears in local mesh for this method. Nevertheless, the opening displacement in the global region is assumed consistently zero based on the overlay method in the BootstrapS-FEM. Therefore,

$$v_{iU}^{G} = -v_{iL}^{G} \tag{2.3}$$

Eq. (2.1), (2.2) and (2.3) are combined to form the total of opening displacement, v_i at the nodes for local region only. The v_i is expressed as

$$v_i = \left(v_{iU}^{G} + v_{iU}^{L}\right) - \left(v_{iL}^{G} + v_{iL}^{L}\right) = v_{iU}^{L} - v_{iL}^{L} \tag{2.4}$$

Calculation of energy release rate is done after calculating the opening displacement at the crack front. Okada [11] introduced the energy release rate, G for the non-symmetrical finite element face arrangement at the crack front. Okada proposed that the energy spent , ΔG_I be calculated at the time of opening of the crack front for the area, S_1 as shown in Figure 2.2. This calculation occurs during the failure mode I in crack growth propagation. This is expressed as

$$\Delta G_I = \frac{1}{2} \int_{S_1} \sigma_{33}(r) v_3(\Delta - r) dS \tag{2.5}$$

Figure 2.2 shows the element's arrangement at the crack front, where Δ and r are the length and width of the element perpendicular and parallel to the crack front mutually, respectively. There are three failure modes namely, mode I, II and III in crack growth propagation. The cohesive stress, σ_{33} in the plane of crack in front with the first subscript 3 illustrates the face that is in vertical direction of the crack front. The second subscript 3 illustrates the axes x_1, x_2 and x_3 as shown in Figure 2.2. The v_i is represented as crack opening displacement function with I direction. Further information about the stress and displacement at the crack face can be referred to Broek [20]. The computation of cohesive stress and displacement function are specified by

$$\sigma_{33}(\bar{r}) = \frac{K_I}{\sqrt{2\pi\bar{r}}}, \quad v_3(\bar{r}) = 4\sqrt{\frac{2\bar{r}}{\pi}} \frac{K_I}{E^1} \tag{2.6}$$

where $E^1 = E$ for the plane stress, and $E^1 = E/\left(1-v^2\right)$ for the plane strain. E and r represent the Young's Modulus and Poisson's ratio of the material properties, respectively. Based on Figure 2.2, $\bar{r}$ is distance from the crack front and θ is angle among the direction of r and normal direction of the crack front. Substituting the stress and displacement into Eq. (2.4) gives

$$\Delta G_I = \int_{\theta_1}^{\theta_2} \int_{0}^{\Delta} \frac{K_I}{\sqrt{2\pi r \cos\phi}} 2\sqrt{\frac{2(\Delta - r)\cos\phi}{}} \frac{K_I}{E^1}(R + r) dr d\theta \tag{2.7}$$

Thus, Eq. (2.7) can be expressed in terms of SIFs of the areas of S_1 and S_2, as shown in Figure 2, by

$$G_I = \frac{K_I^2}{E^1} = \frac{1}{2\left[S_1 - \frac{1}{4}(S_1 - S_2)\right]} \sum_{i=1}^{5} v_i^3 P_i^3 \qquad (2.8)$$

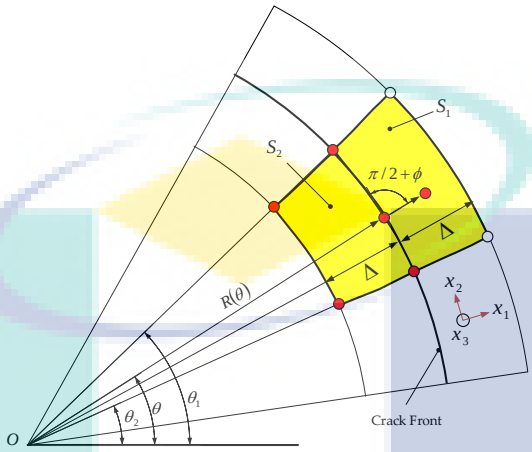

Figure 2: Element arrangement at the crack front of the material

The energy release rate for the remaining failure modes are expressed by

$$G_{II} = \frac{K_{II}^2}{E^1} = \frac{1}{2\left[S_1 - \frac{1}{4}(S_1 - S_2)\right]} \sum_{i=1}^{5} v_i^1 P_i^1 \qquad (2.9)$$

$$G_{III} = \frac{K_{III}^2}{2\mu} = \frac{1}{2\left[S_1 - \frac{1}{4}(S_1 - S_2)\right]} \sum_{i=1}^{5} v_i^2 P_i^2 \qquad (2.10)$$

where μ is shear modulus. Each component of the energy release rate is represented by a subscript at G, whereby the sum of G_I, G_{II} and G_{III} produces G_{Total}. The energy release rate can be changed to SIF, as shown in Eq. (2.8), (2.9) and (2.10). Further details of derivation of element arrangement at crack front can be referred to Okada et. al. [11].

3.0 RESULT AND DISCUSSION

Figure 3 shows a three-dimensional tension model followed by Newman and Raju [21] for verification of the BootstrapS-FEM. The rectangular model is subjected to fatigue loads in tension. The mode I for the SIF along the crack front is calculated and compared for verification purpose.

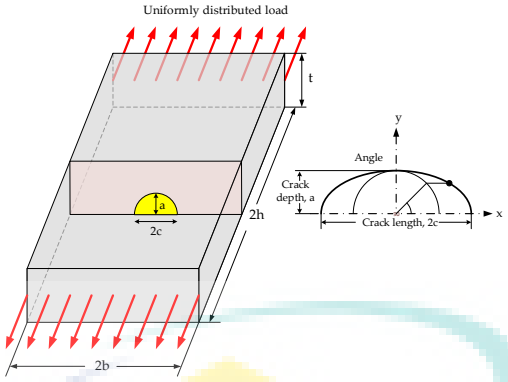

Figure 3: Tension model for surface crack growth.

Two models with different crack shape aspect ratio are examined to show the potential of BootstrapS-FEM when generating the SIF values. The details of the model are shown in Table 3.1.

Table 3.1: Input data for tension models

Tension model	Crack depth, *a* (mm)	Crack length, *c* (mm)	Crack shape aspect ratio, *a/c*		Crack size aspect ratio, *a/t*	Model width aspect ratio, *c/b*	Tension load, Mpa
			Mean	Standard deviation			
A	1	2.5	0.4	0.01	0.2	0.1	10
B	2	2	1.0	0.01	0.2	0.1	10

Tension models A and B have different crack length and crack depth for the semi-elliptical crack shape. Thus, the mean of crack shape aspect ratio for these two models are automatically different. The tension loads applied on these models have equal values. The predictions of SIFs are simulated using BootstrapS-FEM on model A and model B for different crack sizes.

Figure 3.2 and Figure 3.3 show the normalised SIF along the crack front that consists of Newman-Raju, deterministic S-FEM and BoostrapS-FEM. The SIF values are simulated for tension model A and B. The dissimilar of crack shape aspect ratios are simulated in BootstrapS-FEM. This proves that Bootstrap can be simulated with different crack sizes. These ratios are assigned to the crack shape aspect ratios of 0.4 and 1.0 for tension models A and B, respectively, which are expected in different curve types. The SIF is computed based on Eq. (2.8) in VCCM approach. The results of SIF are generalised using the normalisation equation by $Q(a/c)\sqrt{\pi a}$. The $Q(a/c)$ is the shape factor and the detailed explaination can be referred to in a study by Murakami [22]. The results produced are not influenced by material properties. The results from BootstrapS-FEM also use the normalisation equation for comparison purposes. Eq. 3.1 shows the shape factor

$$Q\left(\frac{a}{c}\right)=\sqrt{\int_0^{\pi/2}\left[1-\left(1-\frac{a^2}{c^2}\right)\sin^2\theta\right]^{1/2}d\theta}\approx 1+1.464\left(\frac{a}{c}\right)^{1.65} \qquad (3.1)$$

Figure 3.2 shows the comparison of normalised SIF values for tension model A along the crack front. The SIF curve at the crack front is created using BoostrapS-FEM to be compared with Newman and Raju [21] numerical solution and deterministic S-FEM solution in Figure 3.2 and Figure 3.3. The results of Newman-Raju and deterministic S-FEM are construted in a graph with aspect ratio value for tension model A. BootstrapS-FEM was simulated for the one hundred samples of SIF with mean and standard deviation crack aspect ratio of 0.4 and 0.01, repectively. The crack aspect ratio was distributed in Gaussian distribution. The mean of BootstrapS-FEM was calculated from the hundred samples. The bounds were computed based on minimum and maximum values from the hundred samples of BootstrapS-FEM.

As shown in Figure 3.2, the SIF values reach higher at $2\phi/\pi = 1$ than at 0. This proves that the results from numerical calculations are reasonable. The behaviour of SIF from the mean BootstrapS-FEM agrees well with the Newman-Raju solution. The mean BootstrapS-FEM demonstrates a marginal difference between the solution from Newman-Raju. This is impacted by modelling of the uncertainties in the analysis. The angle $2\phi/\pi = 0$ to 0.6, the SIF of mean BootstrapS-FEM starts increasing and slightly decreasing on the SIFs of Newman-Raju solution. The deterministic S-FEM solution has a slightly decreasing trend from Newman-Raju solution. Figure 3.2 shows 95% confidence bounds for the mean BoostrapS-FEM of the hundred samples. The Newman-Raju solution are within the 95% confidence bounds of upper limit and lower limit for the mean BootstrapS-FEM. This considerably agrees with the Newman-Raju solution because its SIFs are within the bounds of BootstrapS-FEM. The SIF from BootstrapS-FEM is considered valid for the prediction.

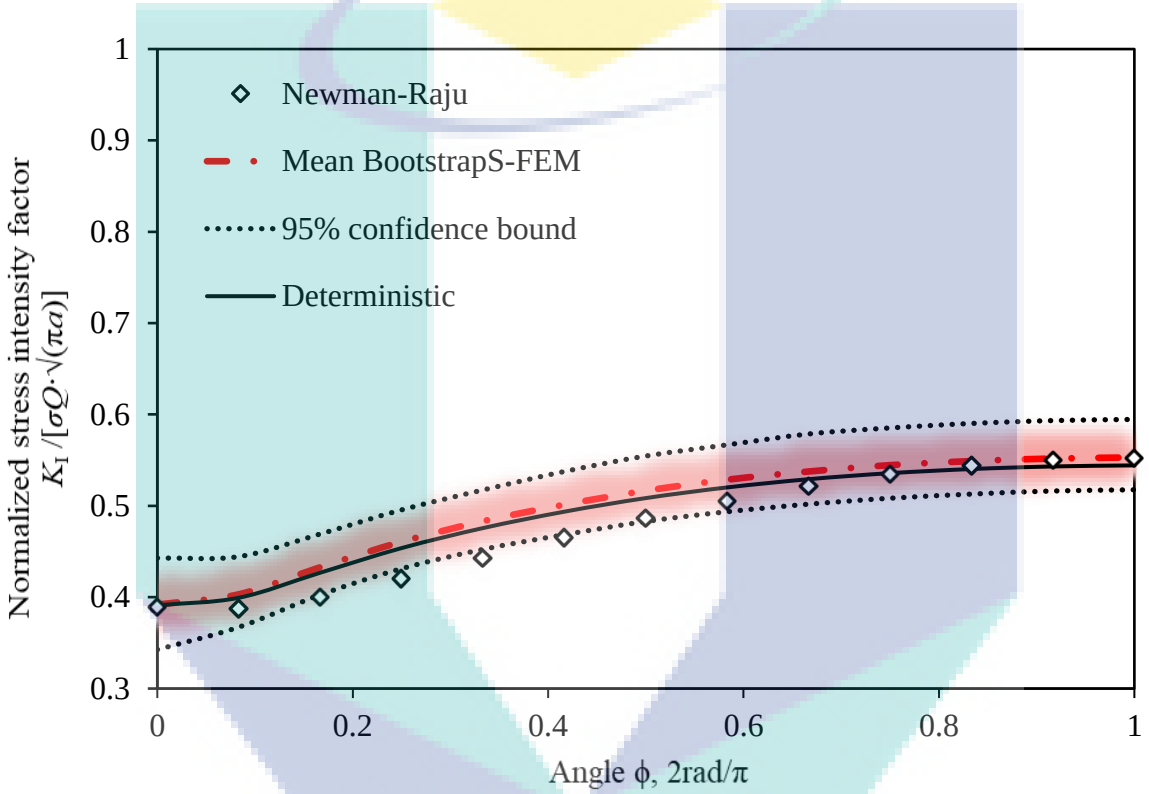

Figure 3.2: Normalised SIFs along the crack front (a/c = 0.4) for tension model A with 95% lower and upper confidence bounds

Figure 3.3 shows the comparison of normalised SIF for tension model B along the crack front. The crack aspect ratio for tension model B is different with tension model A when the angle is increased to 1.0. The crack size and model width aspect ratio for tension model B are retained the same as with tension model A. The tension load applied on tension model B is the same as that applied on model A based on Table 3.1. The difference of aspect ratio is used to verify the prediction of the SIFs by the BootstrapS-FEM. The computation of SIFs are compared with Newman and Raju [21] and the deterministic S-FEM solutions. The hundred samples results of normalised SIF for the mean BoostrapS-FEM are plotted in Figure 3.3. The mean and standard deviation of the crack aspect ratio are used as 1.0 and 0.01, respectively.

The mean Bootstrap-FEM shown in Figure 3.3 includes the 95% confidence bounds for the upper bound and lower bounds. The results of deterministic S-FEM and Newman-Raju solutions are plotted in Figure 3.3 for comparison of SIF. The comparison shows that the mean of BootstrapS-FEM is slightly different with the numerical Newman-Raju solution. The mean BootstrapS-FEM is closer than

deterministic S-FEM between Newman-Raju solution. The SIF of Newman-Raju is located within the 95% confidence bounds of mean BootstrapS-FEM, except at $2\phi/\pi = 0$. Thus, the prediction of SIF by mean BootstrapS-FEM agrees well with the Newman-Raju solution.

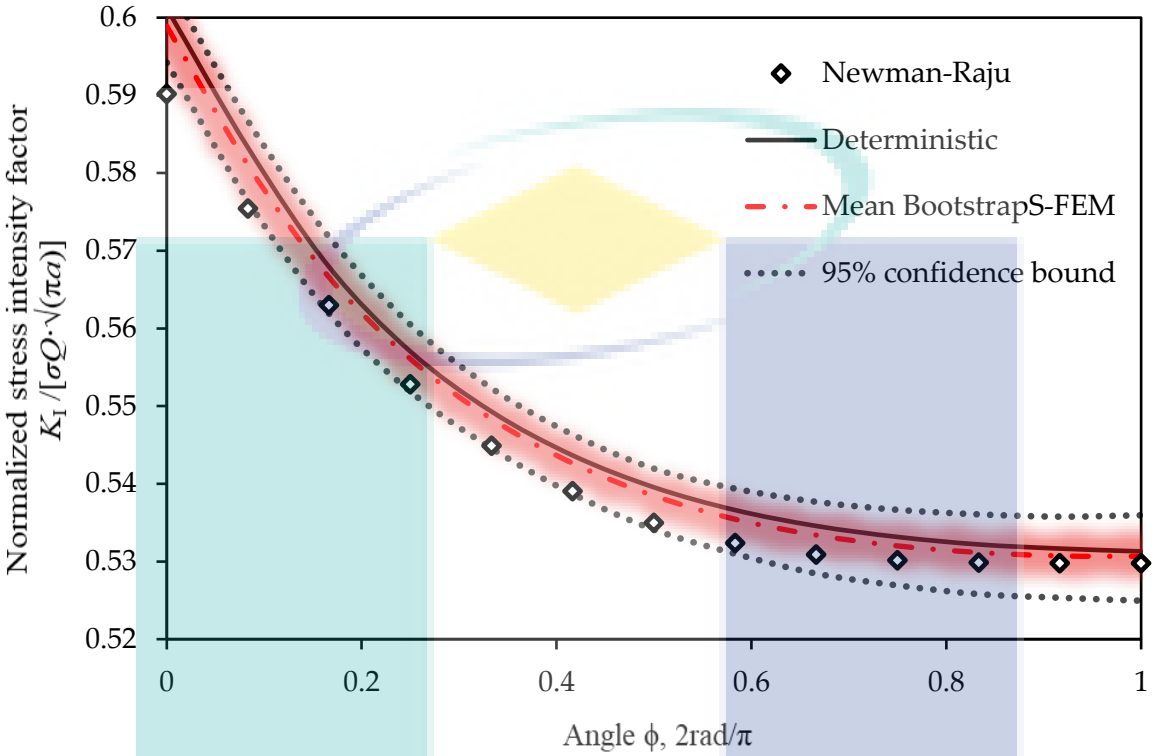

Figure 3.3: Normalised SIFs along the crack front (a/c = 1.0) for tension model B with 95% lower and upper confidence bounds.

The prediction of SIF by BootstrapS-FEM for tension model A and B are validated in Figure 3.2 and Figure 3.3, respectively. They are shown to be in agreement with other deterministic numerical computations namely, deterministic S-FEM and Newman-Raju solution.

4.0 CONCLUSION

The SIF are vital issues that occur in crack growth propagation. Thus, the prediction of SIF by S-FEM is useful with embedded bootstrap resampling method. The SIF is analysed and validated by deterministic S-FEM and Newman-Raju solution. The prediction results of SIFs by BootstrapS-FEM for different crack shape factor are in good agreement with deterministic S-FEM and Newman-Raju solution. The BootstrapS-FEM of SIF predictions are considered valid because the deterministic S-FEM and Newman-Raju solution lay within the 95% confidence bounds. The mean and bounds produced by the BootstrapS-FEM show that there is an augmentation in the prediction of SIF.

ACKNOWLEDGMENTS

This study was funded by RDU170383 from Universiti Malaysia Pahang (UMP) and Fundamental Research Grant Scheme (FRGS/1/2017/TK03/UMP/02/24) from Kementerian Pendidikan Malaysia (KPM) with number RDU170124.

REFERENCES

[1] K. Tazoe, S. Hamada, and H. Noguchi, "Fatigue crack growth behavior of JIS SCM440 steel near fatigue threshold in 9-MPa hydrogen gas environment," *Int. J. Hydrogen Energy*, vol. 42, no. 18, pp. 13158–13170, 2017.

[2] D. F. C. Peixoto and P. M. S. T. de Castro, "Fatigue crack growth of a railway wheel," *Eng. Fail. Anal.*, vol. 82, pp. 420–434, 2017.

[3] S. Mikheevskiy, S. Bogdanov, and G. Glinka, "Analysis of fatigue crack growth under spectrum loading – The UniGrow fatigue crack growth model," *Theor. Appl. Fract. Mech.*, vol. 79, pp. 25–33, 2015.

[4] W. Dong, X. Zhou, and Z. Wu, "A fracture mechanics-based method for prediction of cracking of circular and elliptical concrete rings under restrained shrinkage," *Eng. Fract. Mech.*, vol. 131, pp. 687–701, 2014.

[5] H. W. Reinhardt and O. Mielich, "A fracture mechanics approach to the crack formation in alkali-sensitive grains," *Cem. Concr. Res.*, vol. 41, no. 3, pp. 255–262, 2011.

[6] C. Sarrado, A. Turon, J. Costa, and J. Renart, "On the validity of linear elastic fracture mechanics methods to measure the fracture toughness of adhesive joints," *Int. J. Solids Struct.*, vol. 81, pp. 110–116, 2016.

[7] S. Kashef *et al.*, "Fracture mechanics of stainless steel foams," *Mater. Sci. Eng. A*, vol. 578, pp. 115–124, 2013.

[8] P. Abachi and K. Purazrang, "The correlation between fracture mechanics parameters and creep crack growth rate of Al 7050-T73651 at elevated temperature," *Eng. Fract. Mech.*, vol. 142, pp. 276–286, 2015.

[9] M. Nejati, A. Paluszny, and R. W. Zimmerman, "On the use of quarter-point tetrahedral finite elements in linear elastic fracture mechanics," *Eng. Fract. Mech.*, vol. 144, pp. 194–221, 2015.

[10] R. Krueger, "Virtual crack closure technique: History, approach, and applications," *Am. Soc. Mech. Eng.*, vol. 57, p. 2, 2004.

[11] H. Okada, M. Higashi, M. Kikuchi, Y. Fukui, and N. Kumazawa, "Three dimensional virtual crack closure-integral method (VCCM) with skewed and non-symmetric mesh arrangement at the crack front," *Eng. Fract. Mech.*, vol. 72, no. 11, pp. 1717–1737, 2005.

[12] S. Z. Feng and W. Li, "An accurate and efficient algorithm for the simulation of fatigue crack growth based on XFEM and combined approximations," *Appl. Math. Model.*, vol. 55, pp. 600–615, 2018.

[13] P. O'Hara, C. A. Duarte, and T. Eason, "A two-scale generalized finite element method for interaction and coalescence of multiple crack surfaces," *Eng. Fract. Mech.*, vol. 163, pp. 274–302, 2016.

[14] I. Babuška and B. Q. Guo, "The h, p and h-p version of the finite element method; basis theory and applications," *Adv. Eng. Softw.*, vol. 15, no. 3, pp. 159–174, 1992.

[15] L. Yi and B. Guo, "Superconvergence of the h-p version of the finite element method in one dimension," *J. Comput. Appl. Math.*, vol. 233, no. 2, pp. 150–164, 2009.

[16] M. Kikuchi, Y. Wada, Y. Shintaku, K. Suga, and Y. Li, "Fatigue crack growth simulation in heterogeneous material using s-version FEM," *Int. J. Fatigue*, vol. 58, pp. 47–55, 2014.

[17] M. Kikuchi, Y. Wada, Y. Shimizu, and Y. Li, "Crack growth analysis in a weld-heat-affected zone using S-version FEM," *Int. J. Press. Vessel. Pip.*, vol. 90–91, pp. 2–8, 2012.

[18] M. Kikuchi, Y. Wada, and Y. Li, "Crack growth simulation in heterogeneous material by S-FEM and comparison with experiments," *Eng. Fract. Mech.*, vol. 167, pp. 239–247, 2016.

[19] K. Suga, M. Kikuchi, Y. Wada, and H. Kawai, "Study on fatigue growth of multi-surface flaws in shaft under rotary bending by S-FEM," *Eng. Fract. Mech.*, vol. 174, pp. 207–214, 2017.

[20] D. Broek, *Elementary engineering fracture mechanics*, 1st ed. Springer Netherlands, 1982.

[21] J. C. Newman and I. S. Raju, "An empirical stress-intensity factor equation for the surface crack," *Eng. Fract. Mech.*, vol. 15, no. 1, pp. 185–192, 1981.

[22] Y. Murakami, "Analysis of stress intensity factors of modes I, II and III for inclined surface cracks of arbitrary shape," *Eng. Fract. Mech.*, vol. 22, no. 1, pp. 101–114, 1985.

Bab 3

Statistical Distribution for Prediction of Stress Intensity Factor Using Bootstrap S-version Finite Element Model

M.N.M. Husnain[1], M.R.M. Akramin[1], Z.L. Chuan[2], K. Rozieana[2]

[1]*Faculty of Mechanical & Manufacturing Engineering,*
Universiti Malaysia Pahang, 26600 Pekan,
Pahang Darul Makmur, Malaysia.

[2]*Faculty of Industrial Sciences & Technology,*
Universiti Malaysia Pahang, Lebuhraya Tun Razak, 26300 Gambang,
Pahang Darul Makmur, Malaysia.

Corresponding Author's Email: [1]husnainoh94@gmail.com.my

ABSTRACT

Stress intensity factor (SIF) is one of the most fundamental and useful parameters in all of fracture mechanics. The SIF describes the stress state at a crack tip, is related to the rate of crack growth, and used to establish failure criteria due to fracture. The SIF is determined to define whether the crack will grow or not. The aims of this paper is to examine the best sampling statistical distributions in SIF analysis along the crack front of a structure. Box-Muller transformation is used to generate the statistical distributions which is in normal and lognormal distributions. This method transformed from the random number of the variables within range zero and one. The SIFs are computed using the virtual crack-closure method (VCCM) in bootstrap S-version finite element model (BootstrapS-FEM). The normal and lognormal distributions are represented in 95% of confidence bounds from the one hundred of random samples. The prediction of SIFs are verified with Newman-Raju solution and deterministic S-FEM in 95% of confidence bounds. The prediction of SIFs by BootstrapS-FEM in different statistical distribution are accepted because of the Newman-Raju solution is located in between the 95% confidence bounds. Thus, the lognormal distribution for SIFs prediction is more acceptable between normal distributions.

Keywords

Stress intensity factor; Statistical distributions; Box-Muller transformation; Random samples; Regression analysis

1. Introduction

Defects on the material are essential to investigate because it caused the catastrophic failure. It became critical points for the fatigue strength and lifetime of the materials component. Defects have potential sites for crack initiation from the surface crack growth. Thus, it is caused failure of the component structure. The stress concentration is occurred at the surface defects that leads to inhomogeneous stress field. Nevertheless, the endurance limit of the materials is explored from fatigue tests with un-notched materials specimen. In this condition, the stress concentration is in homogenous stress field with critical cross section [1]. The SIF is important to define because it can affected the crack growth propagation. Fracture mechanics is introduced SIF parameter in crack growth problems.

Fracture mechanics is used to study of the propagation of crack in the materials structures. The investigation of crack propagation is useful based on the fracture mechanics. It can evaluate the long term performance by using the different materials [2], [3]. The method from fracture mechanics is used with several theoretical and parametric applications. Ability of this method is to predict the influence of different mechanical, geometrical and microstructural parameters in its definition [4]. The failure time is obtained through integration of crack speed. By using different fracture mechanics test types, it is give more affected when compared with environment performance on an initiation time or crack speed basis. The experiment was conduct to investigate the lifetime based on fracture mechanics. The data from it is analysed in terms of the SIF at the crack tip for any given crack size. Linear elastic fracture mechanics (LEFM) is assumed that the material in isotropic and linear elastic. The stress field near the crack tip is computed based on the theory of elasticity.

LEFM is the concept or theory in the all energy dissipation that is related with the fracture process. It is showed that the deformation is occurred in linear elastic region but not in

plasticity region. SIF is defined as a function applied stress, specimen geometry and crack length. However, the LEFM concept is becomes invalid when the size of plastic zone at the crack tip becomes large compared to the crack length or the remaining life [5]. LEFM supposed that a linear elastic body is consisted a sharp crack. So, LEFM is described about the energy change that occurs in the linear elastic body can go through a large or increase in crack area. It is means that the fracture increases as the crack size grows to propagate the crack [6]. The virtual crack closure method (VCCM) is used to calculate the SIF based on the LEFM.

The VCCM is suitable for the applications with p-version of the finite element method to compute mixed mode energy release rates. The method provides one global total energy release rate as global forces on a structural level are multiplied with global deformations. This way is calculate the energy available to advance the crack. The total energy release rate is computed locally at the crack front. An additional computation, the stiffness matrix of the elements is involved in calculation that affected by the virtual crack extension. The method is yields the total energy release rate as a function of the direction in which the crack was extended virtually. The yielding information depends on the growth direction [7]. The Finite Element Method (FEM) software is complicated to develop that depends on the theory, implementation aspect, computational experience and engineering. It is related with computer hardware and manpower cost to solve by engineering community [8], [9]. FEM is applied to LEFM to generated suitable mesh for crack model in 2-dimensional or in multiple cracks. The interaction integrals is formulated which to applied in different types of the materials [20].

The existing integrals infinite element is used for linear hyperbolic problems including simple element such as triangular and quadrilateral element in 2-dimensional. FEM is allowed to use the general polygonal or polyhedral meshes which helpful features in adaptive mesh refinements. FEM is come up with a symmetric and positive definite system [10]. The singular stress field is created by refining mesh at the crack tip or using special types of elements such as quarter point elements [11]. A suitable mesh is handled by advanced re-meshing algorithms. The fine mesh is used at the vicinity of the crack tip and crack front so that the singular stress field is determined accurately [12]. The extended version is applied to improve the quality of FEM calculations by using the existing adaptive techniques such as h-version and p-version. The combination of two methods are produced the S-version method which is increased a polynomial order and finer mesh.

By using the S-version, the problems are solved significantly and give more impact in program of engineering development. Especially, the program STRIPE (Aeronautical Research Institute of Sweden), Applied Structure (Rasna Corp., California, USA), PHLEX (Computational Mechanics, Texas, USA) and MSC/PROBE (MacNeal Schwendler, California, USA) [8]. The mathematical theorem is important to conduct the software in two and three dimensional model [13], [14]. There are many major commercial based on the h-version of FEM such as MSCNASTRAN, ADINA, ANSYS and etc. There are only two of commercial programs such as FIESTA and MSCPROBE based on p-version and hp-version [15]. Thus, SIF is evaluated along the crack front. The calculation of SIF is required great computational effort due to geometry modeling of the crack growth propagation. Kikuchi et al. is developed combination of S-FEM and auto-meshing method to simulate the fatigue crack growth [16]. Probabilistic method is useful to predict the SIF in hundreds random of samples. It is avoided from the scatter prediction of SIFs.

The probabilistic is defined the input parameters as distributions and predict the output of distributions and bounds of performance [17]. The types of distributions are normally used such as normal, lognormal, Weibull distributions and etc. The data of the crack growth can used to estimate in the types of distributions [18], [19]. In the commercial software, the probabilistic simulation is widely used in the ABAQUS software. The distribution is randomly generated by using the distribution function based on the determined parameters [17], [18]. Thus, the probabilistic method is widely applied in the engineering studies.

See that failure by fracture include the growth of cracks it created that monitoring the size of a crack in a specific structure give a method for evaluating quantitatively the strength before failure completely. The stress analysis was carried out from the BootstrapS-FEM and the parameters of fracture mechanics were computed. The prediction of SIFs are simulated in BootstrapS-FEM based on the statistical distribution between normal and lognormal distributions. The SIFs are compared between numerical Newman-Raju solution and deterministic S-FEM.

2. Methodology

This section is explaining the principle of generating normal and lognormal distributions using Box-Muller transform algorithm. The normal and lognormal distributions are developed from the random samples using the Box Muller transformation method. The SIFs value is predicted by BootstrapS-FEM for one hundred of random samples. The SIF and energy release rate are the parameters that will figured out

the crack growth in LEFM. The fracture parameters are predicted by using VCCM method.

2.1 Box-Muller Transform Algorithm

Box and Muller [21] proposed another efficient transform algorithm. This method is generated two independent samples from a standard normal distribution. Their proposed Box-Muller transformation algorithm is competent to sample bivariate Standard Gaussian random variables, $Z_j \sim N(z_j;0,1)$ and $Z_k \sim N(z_k;0,1)$ where Z_j and Z_k are two independent random variables. Suppose that $X_j \sim U(x_j;0,1)$ and $X_k \sim U(x_k;0,1)$ are two independent uniform random variables with $X_j \in \lfloor x_j \rfloor_N$, $X_k \notin [x_k]_N$; $j.k = 1,2,3,...,N$ and $x_j, x_k \in [0,1]$. In addition, suppose that the relationship between x_j, x_k, z_j and x_k can be expressed as

$$x_j = \exp\left(-\frac{\left(z_j^2 + z_k^2\right)}{2}\right) \tag{2.1}$$

$$x_k = \frac{1}{2\pi}\tan^{-1}\left(\frac{z_k}{z_j}\right) \tag{2.2}$$

By applying the change-of-variable techniques, the joint probability density function (PDF) corresponds to two independent Standard Gaussian random variables, $f(z_j, z_k)$ is resulted as follows.

$$f(z_j, z_k) = f\left(x_j(z_j, z_k), x_k(z_j, z_k)\right)\left|\frac{\partial(x_j, x_k)}{\partial(z_j, z_k)}\right| \tag{2.3}$$

The cumulative distribution function is

$$f(z_j, z_k) = \frac{1}{\sqrt{2\pi}}\exp\left(-\frac{z_j}{2}\right)\frac{1}{\sqrt{2\pi}}\exp\left(-\frac{z_k}{2}\right) \tag{2.4}$$

The idea behind the Box-Muller transform is to imagine two independent samples $Z_j, Z_k \sim N(0,1)$ are plotted in the Cartesian plane as shown in Figure 2.1. This is represented as a polar coordinates which it needed the distance, R between (Z_j, Z_k) and the origin along with the angle, θ in x-axis.

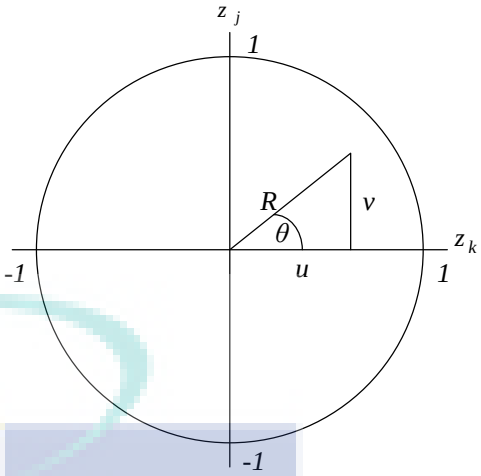

Fig. 2.1: Polar form in the Cartesian plane

The equation is presented from the origin, $R = \sqrt{Z_j{}^2 + Z_k{}^2}$ and simplified to $R^2 = Z_j{}^2 + Z_k{}^2$. The polar coordinates for two independent standard normal by converting back to Cartesian as

$$Z_j = R\cos\theta \tag{2.5}$$

$$Z_k = R\sin\theta \tag{2.6}$$

where $R = \sqrt{-2\log x_j}$ and $\theta = 2\pi x_k$.

Eq. (2.4) consolidated that the Eq. (2.2) and Eq. (2.3) is competent to transform variables X_j and X_k into Z_j and Z_k respectively. By manipulating Eq. (2.2) and Eq. (2.3), both equations can be rewritten based on Eq. (2.5) and Eq. (2.6) as

$$z_j = \sqrt{-2\log(x_j)}\cos(2\pi x_k) \tag{2.7}$$

$$z_k = \sqrt{-2\log(x_k)}\cos(2\pi x_j) \tag{2.8}$$

Where $\partial(.)$ represents the partial derivative function and $\log(.)$ represents the natural logarithm function. Since this study merely focused on univariate random variable, therefore the efficiency of Eq. (2.7) and Eq. (2.8) of the transformation algorithms are evaluated, respectively.

2.2 Transformation a Standard Normal Random Variable into Gaussian and Lognormal Random Variable

Based on Table 3.1, the mean and standard deviation for the crack aspect ratio are used in transform normal and lognormal as $(a/c) \sim N(\mu, \sigma^2)$. Therefore, transforming the Standard Gaussian random variables into a Gaussian random variables is indeed much needed. The Gaussian random variables is resulted when the rules for transforming Gaussian random variables is applied, including scalar multiplication and adding a constant. In mathematics,

$$(a/c)_N = \mu + z\sigma \tag{2.9}$$

Based on the probability theory, the lognormal random variables are resulted from taking exponential of Eq. (2.9), such that

$$(a/c)_L = \exp(z) \tag{2.10}$$

2.3 Virtual Crack Closure Method (VCCM)

The SIFs are calculated based on the energy release rate, G using the VCCM. The Eq. (2.11) can be expressed in terms of the SIFs of the areas of S_1 and S_2, as shown in Figure 2.2, by

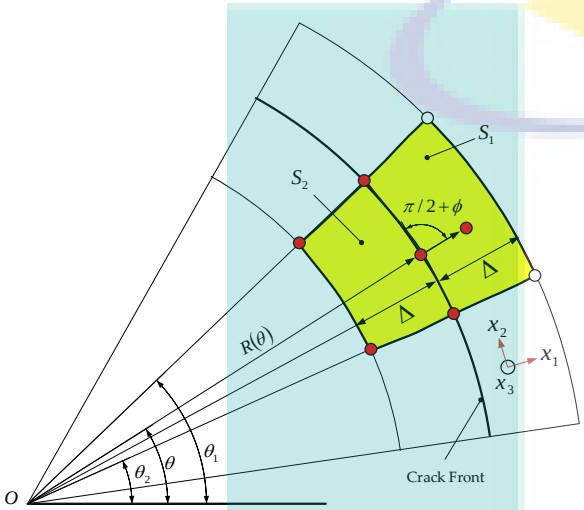

Fig. 2.2: Element arrangement at the crack front

$$G_1 = \frac{K_I}{E'} = \frac{1}{2\left[S_1 - \frac{1}{4}(S_1 + S_2)\right]} \sum_{i=1}^{5} v_i^3 P_i^3 \tag{2.11}$$

The energy release rate for the remaining failure modes are expressed by

$$G_{II} = \frac{K_{II}^2}{E'} = \frac{1}{2\left[S_1 - \frac{1}{4}(S_1 + S_2)\right]} \sum_{i=1}^{5} v_i^1 P_i^1 \tag{2.12}$$

$$G_{III} = \frac{K_{III}^2}{2\mu} = \frac{1}{2\left[S_1 - \frac{1}{4}(S_1 + S_2)\right]} \sum_{i=1}^{5} v_i^{21} P_i^2 \tag{2.13}$$

Where μ is the shear modulus. Each component of the energy release rate is represented by a subscript at G, whereby the sum of G_I, G_{II} and G_{III} produces G_{Total}. The energy release rate can be changed to the SIF, as shown in Eqs. (2.11), (2.12) and (2.13). For further details of derivation of element arrangement at crack front can be referred to Okada et. al. [11].

3. Result and Discussion

The BootstrapS-FEM generates the normal and lognormal distribution for one hundred of samples. The value of SIFs are computed based on the Eq. (2.11) for mode I crack growth propagation. Figure 3.1 shows the three-dimensional model that subjected to tension load with semi-elliptical crack shape. The model was used for verification of SIF between BootstrapS-FEM and Newman & Raju [22]. The comparison of SIF was represented in two different distributions which is normal and lognormal distribution.

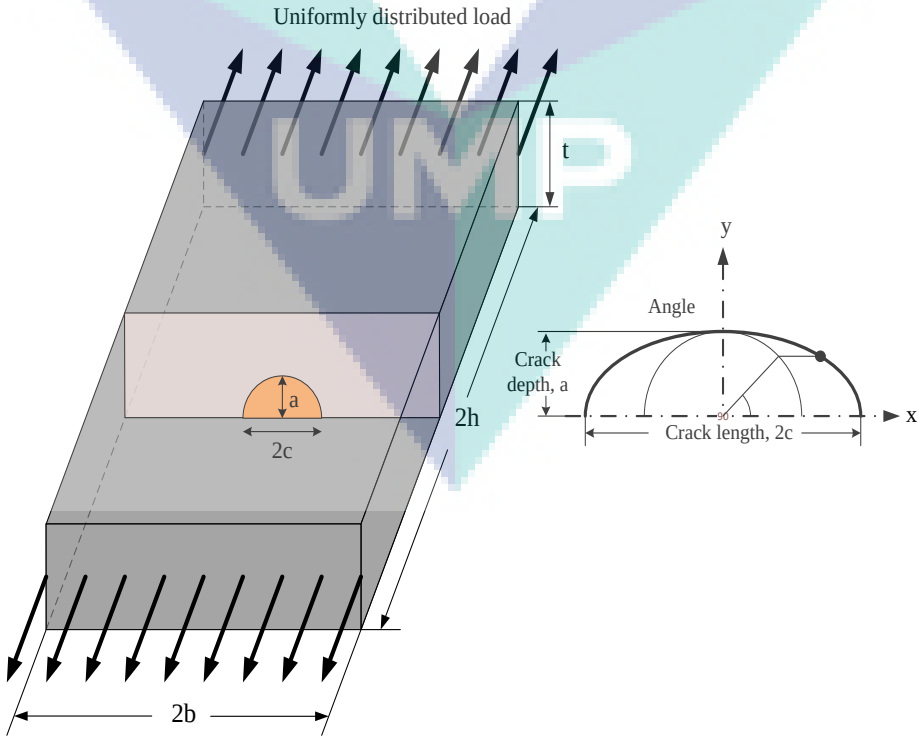

Fig. 3.1: Comparison of normalised SIFs along the crack front

Table. 3.1: Details parameter of the model.

Crack depth, *a (mm)*	Crack length, *c (mm)*	Crack shape aspect, ratio, *a/c*		Crack size aspect ratio, *a/t*	Model width aspect ratio, *c/b*	Tension load, *MPa*
		Mean	Standard deviation			
1	2.5	0.4	0.01	0.2	0.1	10

The model was considered to show the ability of the BootstrapS-FEM in producing SIF values. Thus, the prediction of SIFs results are compared with numerical method Newman-Raju solution. The parameter details of the model is shown in Table 3.1.

Figure 3.2 shows the comparison of the normalised SIFs along the crack front for the tension model. The SIF curve that constructed using the BootstrapS-FEM with the numerical solution by Newman & Raju [22] and deterministic S-FEM. The BootstrapS-FEM was generated in Gaussian and lognormal distribution. Two means of BootsrapS-FEM was represented in Figure 3.2 for distinguish the distributions. The means of the BootsrapS-FEM were constructed build upon a 100 samples.

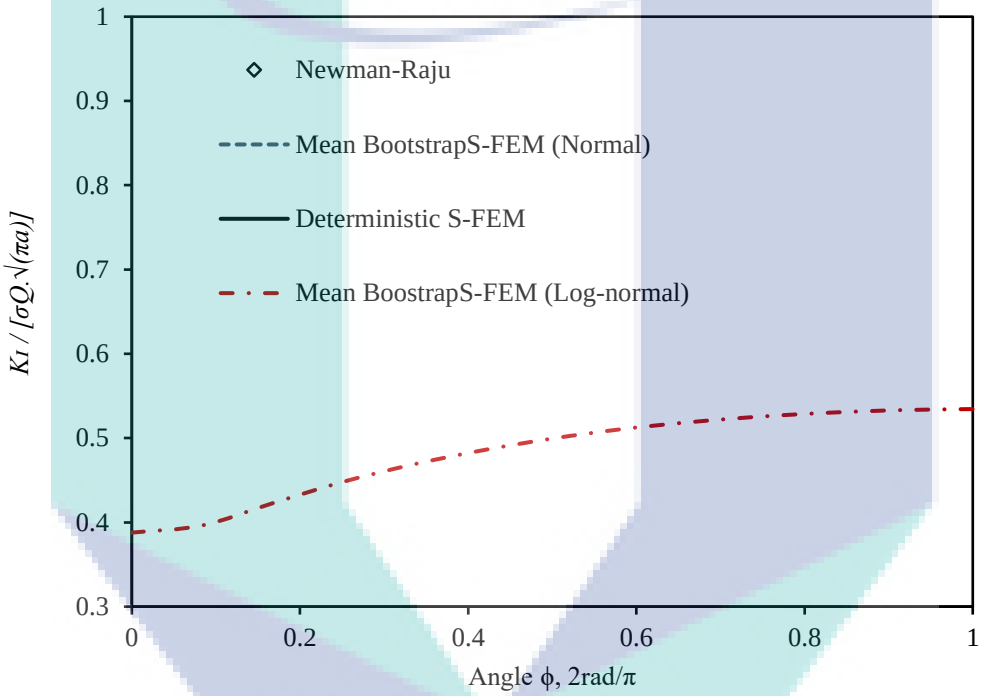

Fig. 3.2: Comparison of normalised SIFs along the crack front

Figure 3.3 shows the results of the normalized SIFs by the Newman-Raju solution and mean BootstrapS-FEM in normal distribution. The bounds in Figure 3.3 had a 95% confidence interval based on the maximum and minimum 100 samples of SIFs. The 95% of confidence bounds are the range within which 95% of the result of BoostrapS-FEM in normal distribution can be defined. The SIFs of Newman–Raju solution was located inside the 95% confidence bounds of upper limit and lower limit for mean BootstrapS-FEM (Normal). This was significantly agreed with the Newman-Raju solution because the points falls within the range of 95% bounds by BootstrapS-FEM. Furthermore, the prediction of SIFs by BoostrapS-FEM (Normal) examined valid based on the 95% confidence bounds

The mean BoostrapS-FEM of normalized SIFs for lognormal statistical distribution are shown in Figure 3.4 including the 95% confidence bounds. The results are compared with Newman-Raju solution for validation process as a prediction. The comparison shows that the mean of BootstrapS-FEM (Lognormal) slightly contrasting between numerical Newman-Raju solution. The mean of BoostrapS-FEM (Lognormal) is more closer than BostrapS-FEM (Normal) towards Newman-Raju solution. The SIFs of Newman-Raju solution is discovered inside the 95% confidence bounds of the mean BootstrapS-FEM (Lognormal). Thus, the estimation of SIFs by the mean BootstrapS-FEM is agreed with the Newman-Raju solution

.

Based on the Figure 3.3 and Figure 3.4, the 95% confidence bounds of the BootstrapS-FEM (Lognormal) is narrower than the BootstrapS-FEM (Normal) which is slightly wider. As a consequence, boths BootstrapS-FEM of SIFs predictions are valid because the numerical Newman-Raju falls in range of 95% confidence bounds.

The prediction of SIFs by BootstrapS-FEM in normal and lognormal distributions are validated based on the Figure 3.3 and Figure 3.4 respectively. The prediction of SIFs by BootstrapS-FEM in different distribution shows agreement

with the numerical solution Newman-Raju and deterministic S-FEM.

4. Conclusions

The SIFs is the main parameter in analysis process since it will affects the remaining life of structures. Thus, the prediction of SIFs by BootstrapS-FEM is useful for statistical analysis. This paper used normal and lognormal distribution to predict the SIFs along the crack front. The result for both distributions are analysed and validated by Newman-Raju solution and deterministic S-FEM. The Bootstrap (Normal) and BootstrapS-FEM (Lognormal) are considered valid based on the 95% confidence bounds. The Newman-Raju solution is indicated in between the 95% confidence bounds. Furthermore, the best distribution by BootstrapS-FEM is lognormal distribution. The lognormal distribution is more accurate than normal distributions around one percent error differences against Newman-Raju solution.

5. AcknowledgEment

This study was funded by RDU170383 from Universiti Malaysia Pahang (UMP) and Fundamental Research Grant Scheme (FRGS/1/2017/TK03/UMP/02/24) from Kementerian Pendidikan Malaysia (KPM) with number RDU170124.

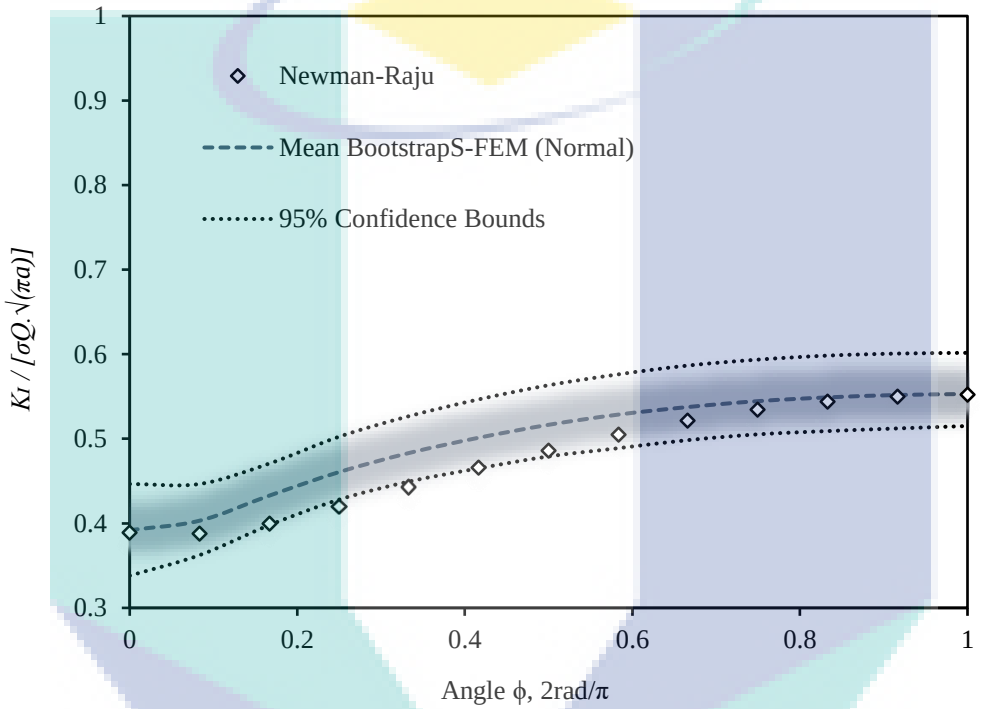

Fig. 3.3: Normalised SIFs along the crack front for normal distribution with 95% upper and lower bound

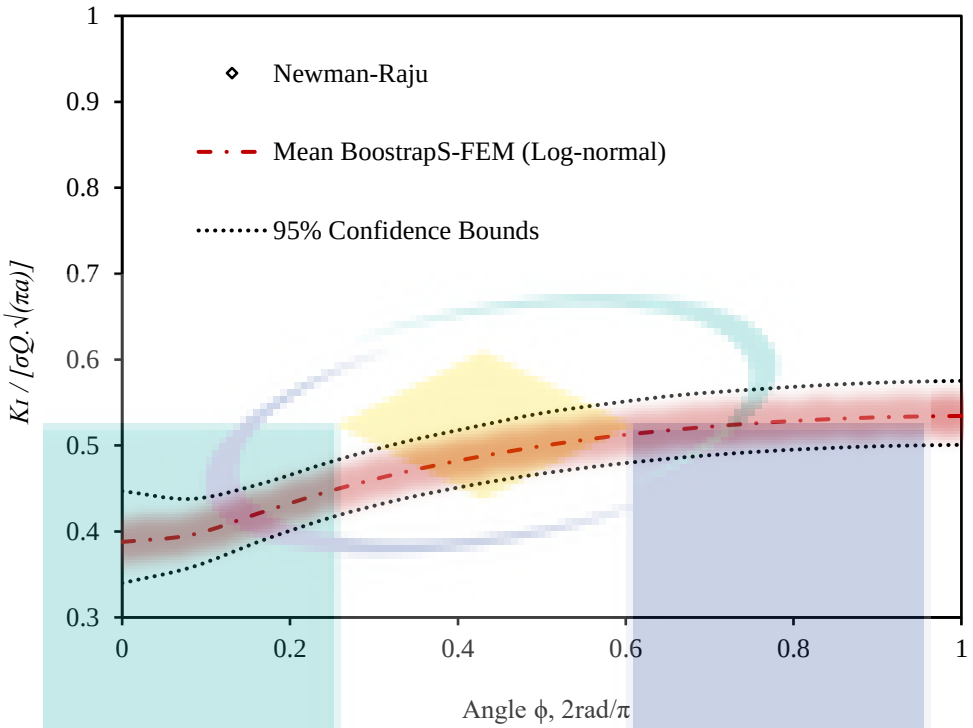

Fig. 3.4: Normalised SIFs along the crack front for lognormal distribution with 95% upper and lower bound

References

1. Götz, S., F. Ellmer, and K.G. Eulitz, *A fracture mechanics-based approach to estimating the endurance limit of notched components.* Engineering Fracture Mechanics, 2016. **151**(Supplement C): p. 37-50.
2. Andena, L., et al., *A fracture mechanics approach for the prediction of the failure time of polybutene pipes.* Engineering Fracture Mechanics, 2009. **76**(18): p. 2666-2677.
3. Kamaludin, M.A., et al., *A fracture mechanics approach to characterising the environmental stress cracking behaviour of thermoplastics.* Theoretical and Applied Fracture Mechanics, 2017. **92**(Supplement C): p. 373-380.
4. Chapetti, M.D. and L.F. Jaureguizahar, *Fatigue behavior prediction of welded joints by using an integrated fracture mechanics approach.* International Journal of Fatigue, 2012. **43**(Supplement C): p. 43-53.
5. Noraphaiphipaksa, N., et al., *Fretting fatigue life prediction of 316L stainless steel based on elastic–plastic fracture mechanics approach.* Tribology International, 2014. **78**(Supplement C): p. 84-93.
6. Kashef, S., et al., *Fracture mechanics of stainless steel foams.* Materials Science and Engineering: A, 2013. **578**(Supplement C): p. 115-124.
7. Krueger, R., *Virtual crack closure technique: History, approach, and applications.* Applied Mechanics Reviews, 2004. **57**(1-6): p. 109-143.
8. Babuška, I. and B.Q. Guo, *The h, p and h-p version of the finite element method; basis theory and applications.* Advances in Engineering Software, 1992. **15**(3): p. 159-174.
9. Yi, L. and B. Guo, *Superconvergence of the h-p version of the finite element method in one dimension.* Journal of Computational and Applied Mathematics, 2009. **233**(2): p. 150-164.
10. Mu, L. and X. Ye, *A simple finite element method for linear hyperbolic problems.* Journal of Computational and Applied Mathematics, 2018. **330**(Supplement C): p. 330-339.
11. O'Hara, P., C.A. Duarte, and T. Eason, *A two-scale generalized finite element method for interaction and coalescence of multiple crack surfaces.* Engineering Fracture Mechanics, 2016. **163**(Supplement C): p. 274-302.
12. Feng, S.Z. and W. Li, *An accurate and efficient algorithm for the simulation of fatigue crack growth based on XFEM and combined approximations.* Applied Mathematical Modelling.
13. Guo, B. and J. Zhang, *Construction of polynomial extensions in two dimensions and application to the h-pfinite element method.* Journal of Computational and Applied Mathematics, 2014. **261**(Supplement C): p. 249-270.
14. zhang, J. and L. Yi, *The convergence rate of p and h-p FEM for three dimensional elasticity problems on L-shape domain.* Procedia Engineering, 2012. **31**(Supplement C): p. 1024-1032.
15. Babuška, I. and M. Suri, *The p- and h-p versions of the finite element method, an overview.* Computer Methods in Applied Mechanics and Engineering, 1990. **80**(1): p. 5-26.
16. Suga, K., et al., *Study on fatigue growth of multi-surface flaws in shaft under rotary bending by S-FEM.* Engineering Fracture Mechanics.
17. Coombs, D.J., P.J. Rullkoetter, and P.J. Laz, *Efficient probabilistic finite element analysis of a lumbar motion segment.* Journal of Biomechanics, 2017. **61**(Supplement C): p. 65-74.
18. Li, Y., et al., *Shape-instability life scatter prediction of 40Cr steel: Damage-coupled crystal plastic probabilistic finite element method.* International Journal of Plasticity, 2016. **79**(Supplement C): p. 1-18.
19. Qiu, Z. and Y. Zheng, *Fatigue crack growth modeling and prediction with uncertainties via stochastic perturbation series expansion method.* International Journal of Mechanical Sciences, 2017. **134**(Supplement C): p. 284-290.
20. Song, C., E.T. Ooi, and S. Natarajan, *A review of the scaled boundary finite element method for two-dimensional linear elastic fracture mechanics.* Engineering Fracture Mechanics, 2017.
21. Box, G.E.P. and M.E. Muller, *A Note on the Generation of Random Normal Deviates.* Ann. Math. Statist., 1958. **29**(2): p. 610-611.
22. Newman, J.C. and I.S. Raju, *An empirical stress-intensity factor equation for the surface crack.* Engineering Fracture Mechanics, 1981. **15**(1): p. 185-192.

Bab 4

Surface crack growth prediction under fatigue load using the S-version Finite Element Model (S-FEM)

M.N.M. Husnain[1], M.R.M. Akramin[1], Z.L. Chuan[2]

[1] Faculty of Mechanical Engineering, Universiti Malaysia Pahang, 26600 Pekan, Pahang Darul Makmur
[2] Faculty of Industrial Sciences & Technology, Universiti Malaysia Pahang, Lebuhraya Tun Razak, 26300 Gambang, Pahang Darul Makmur
*Corresponding author: husnainoh94@gmail.com

Abstract.
Prediction of fatigue crack growth is one of the important issues to prevent catastrophic failure from damage tolerance perspective. The surface of crack shape usually in semi-elliptical that was maintained during the whole propagation. The aim of this paper is to illustrate the surface crack growth that subjected to fatigue loading. The four-point bending and three point bending have been simulated by using the S-version Finite Element Model (S-FEM). The simulation is conducted for aluminium alloy A7075-T6 and A2017-T3 with all of the parameters based on the previous experiment. The semi-elliptical crack shape is applied during the simulation process to represent with the reality of crack growth phenomena. Paris' Law model approach is presented in fatigue crack growth simulation. The S-FEM produced the surface crack growth and fatigue life prediction. The result of the S-FEM prediction was compared with the previous experiment. The result was presented in a graph for comparison between S-FEM prediction with the experimental result. The S-FEM result obtained is good agreement with the experiment result.

1. Introduction

Defects on the materials such as initial flaws or imperfections in the materials are essential to study seriously. The flaw normally affects mechanical behaviors and structures of materials as defects. Then, the performances and components of the materials are changed naturally. Crack is formed from the flaw in materials structure when applied load. When flaw reaches a critical size, the crack may propagate in this condition. The catastrophic failure is presented in the materials component [1]. Nowadays, an indication of initial flaws is the main source that affecting the structural materials. It is produced by impact for the critical failure in the engineering industries such as automotive, aerospace and others/etc. Initial flaw size of the crack growth is the one of a factor for the failure occurred. The initial flaws size can be modeled to investigate the fatigue life of the materials [2], [3]. The bending model is simulated with the numerical method using the powerful computational tool.

Fatigue crack growth an embedded crack is studied with some parameters such as crack shapes, sizes and stress ratio. It is to investigate the fatigue crack growth behavior of interacting cracks. The crack growth is simulated by using the finite element method (FEM). It is able to characterize an arbitrary crack in FEM with meshing. The initial crack is beginning of degradation at crack initiation. The simulation can meet the criterion of crack initiation when it started [4]. The computational effort becomes very large when the iterations of crack propagation increase. Extended FEM is used to avoid mesh dependent difficulties in the modeling of crack growth problems. It is used as the partition of unity enrichment [5]. The shape function in FEM is enrichment functions. FEM application in LEFM has formed the enrichment function as well as singular crack tip expansion functions. It is used to define the displacement or stress contours with a 3D crack in an elastic medium accurately. The global error is controlled by the quality of local error. If the local error is presented in high enrichment function, it is expected good global accuracy as well [6]. The meshing problems and difficulty of embedded crack shape is resolved with some improvement in FEM.

The extended version can be applied to improve the quality of FEM calculations by using the existing adaptive techniques such as h-version and p-version. The h-method is used for mesh refining and the p-

method is used for increased the polynomial order. The finite element mesh based on the h-method has subdivided the elements in the same order into the small elements. It is purposed to get fine the in the meshing of the elements. The p-method is used to increase the polynomial order approximation in the same mesh [7]. The *p*-version leaves the mesh unchanged and increases the polynomial degree of the shape functions locally or globally [8]. Lastly, the combination for both of them can increase the polynomial degree and mesh refinement. It is called as s-version that has a great advantage to utilized [9], [7], [10]. The s-version has increased the resolution the higher order hierarchical elements by superimposing additional meshes. The s-version is implemented in FEM as S-FEM to solve the various problems. The S-FEM is applied in surface crack growth to know its lifetime and crack propagation based on its parameter [11].

In numerical method, the problem is about meshing process between the model with the initial crack shape. The prediction of fatigue life is difficult to compute when the fracture start propagates and failure. This paper presents the analysis of S-FEM for fatigue surface crack. The aim of this paper is to illustrate the surface crack growth under bending fatigue loads. The fatigue life is computed and presented in this paper simultaneously. The S-FEM is used as a method to solve the fatigue crack growth for the bending model. In this study, the result from the S-FEM simulation for four-point bending and three-point bending is compared with previous researcher's experimental results.

2. Materials

The Aluminium 7075-T6 was used for aircraft parts in the aircraft industry. The 7075 aluminum alloy was an aluminum alloy, with zinc as the primary alloying element. It was strong, with strength comparable to many sheets of steel, and had good fatigue strength and average machinability. The 7075 aluminum alloy's composition roughly includes 5.6 - 6.1 % zinc, 2.1 - 2.5 % magnesium, 1.2 - 1.6 % copper, and less than a half percent of silicon, iron, manganese, titanium, chromium, and other metals. Table 1 shows the parameter detail for four-point bending model of Aluminium 7075-T6.

Table 1. Input for Aluminium alloy 7075-T6 from Ohdama et al. [12].

Variable	Value
Critical stress intensity factor, K_{IC}	29 MPa·√m
Fatigue power parameter, n	2.88
Tensile Strength, Yield	691 MPa
Young's modulus, E	71.7 GPa
Paris coefficient, C	6.54×10^{-13}
Threshold value, ΔK_{th}	5.66 MPa·√m
Maximum crack growth increment, da_{max}	1.3 mm
Initial crack length, c	4.5 mm
Initial crack depth, a	3.5 mm

Aluminium 2017-T3 was used commonly in the manufacture of aircraft components, screw machine products and fittings, pulleys, gauges, coat hangers, and in crochet and knitting needles. The chemical composition of Aluminium 2017-T3 was included 91.5 - 95.5 % aluminium, 3.5 - 4.5 % copper, 0.7 % iron, 0.4 - 1 % manganese, 0.4 - 0.8 % magnesium, 0.2 - 0.8 silicon, 0.25 % zinc, 0.15 % titanium and 0.1 % of chromium. The input detail for Aluminium 2017-T3 three-point bending model is shown in Table 2.

Table 2. Input for the Aluminium alloy 2017-T3 from Kikuchi et al. [13].

Variable	Value
Critical stress intensity factor, K_{IC}	26 MPa·√m
Fatigue power parameter, n	2.93
Tensile Strength, Yield	333 Mpa
Young's modulus, E	70.2 Gpa
Paris coefficient, C	2.66×10^{-10}
Threshold value, ΔK_{th}	6.7 MPa·√m

Initial crack length, *c*	2.85 mm
Initial crack depth, *a*	5.00 mm

3. Methodology

3.1 Four-point bending and three-point bending

The S-FEM concepts were applied in this simulation to analyze the surface crack growth. The semi-elliptical crack shape is introduced at the center of the models [14], [15]. The four-point bending model with 2b = 65 mm, 2h = 160 mm and t = 25 mm was designed and simulated in the S-FEM model was shown in Figure 4 (a). The crack was propagated based on the simulation until the fracture propagated completely. The semi-elliptical crack shape was located at the middle of the specimen model. An initial crack shape aspect is with a = 3.5 mm and 2c = 4.5 mm.

Figure 1 (b) shows the details dimension for geometry of three-point bending of Aluminium 2017-T3 with *2h* = 150 mm, *2b* = 50 mm and *t* = 15 mm. The model was analyzed in S-FEM model based on the fatigue crack growth. The semi-elliptical crack shape as an initial crack was designed with *a* = 5 mm and *2c* = 2.85 mm.

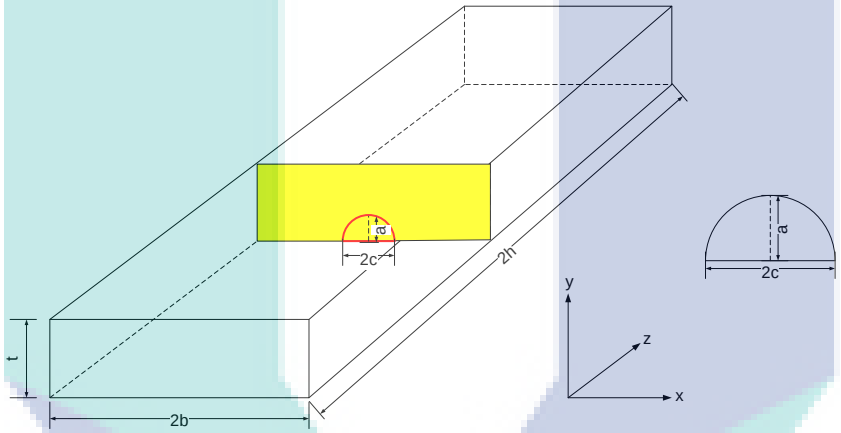

(a) Details dimensions of four-point bending model with semi-elliptical crack shape for Aluminium alloy A7075-T6.

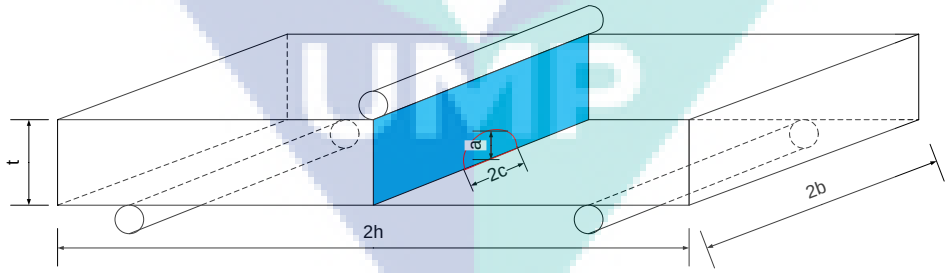

(b) Details dimensions of four-point bending model with semi-elliptical crack shape for Aluminium alloy 2017-T3.

Figure 1. The geometry of four-point bending of (a) and three-point bending of (b).

Figure 2 (a) shows the model for four-point bending in a meshing with a boundary condition. The model had used 0.1 as stress ratio to produce beach marks. The model (a) was conducted with 45 kN as a loading in cyclic load. The use 45kN was ensured that it discovered in fatigue region, which affirmed that the fatigue would occur for the dimensions of this material. The crack shape aspect ratio, *a/c* was 0.8. The three-point bending was shown in Figure 2 (b). The 9 kN as a load was applied repeatedly on the surface

model (b) with a stress ratio also 0.1. The crack aspect ratio, *a/c* for the model (b) was 1.7. The parameters detail was the same as the previous experimental specimen based on Table 1 and Table 2. The model was modeled in S-FEM with input and parameters.

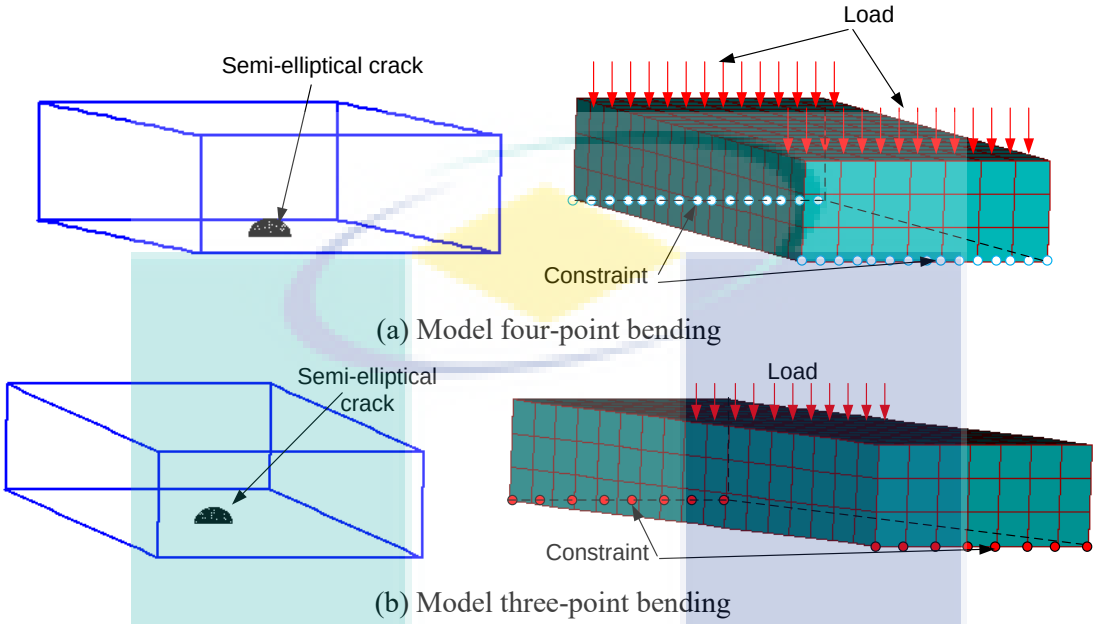

Figure 2. Overlaid local mesh in wireframe view and global mesh with boundary condition.

3.2 S-version Finite Element Model (S-FEM)

The concept of S-FEM was exhibited in Figure 3 that implementation in this surface cracks growth analysis. There were consisted of two parts area such as local and global area. These two parts of the area were important to generate the meshing of the model analysis. The local area was discovered the crack tip meshing and the global area was discovered for the whole model.

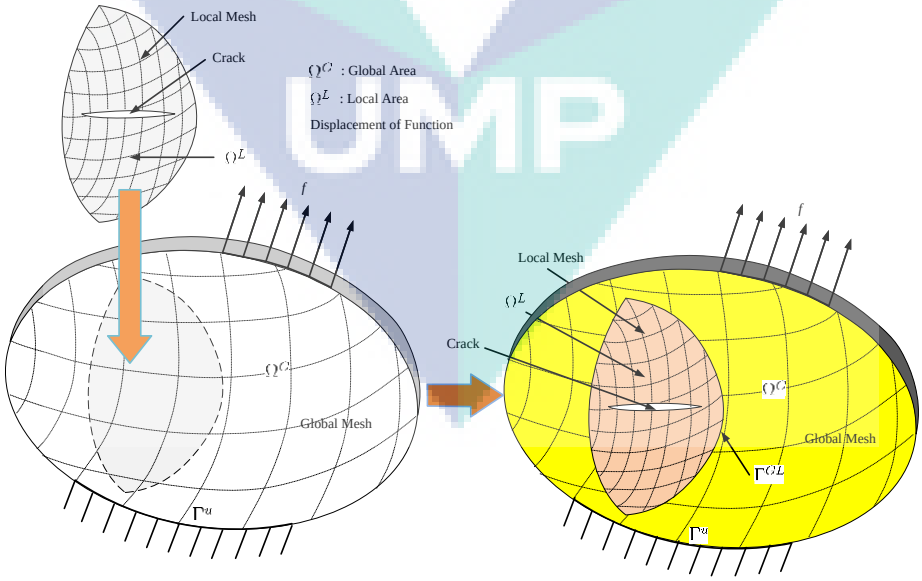

Figure 3. The concept of S-FEM.

The two of parts meshing were combined as followed as S-FEM concept. The different orientation of mesh was produced such as coarser mesh and denser mesh. The local area was generated by coarser mesh and the denser mesh was generated for the global area. The crack tip was discovered by the local area during the creation of the local mesh, Ω^L. The global mesh, Ω^G was produced for the whole global area. The local mesh subsequently was enveloped onto the global mesh. The boundary of each area was represented as Γ. The global area was applied by the boundary of constraint displacement, Γ^u, and the boundary of force, Γ^t. The local area was embedded in the global area is represented as overlay boundary, Γ^{GL}. The overlay boundary was examined to compute the displacement of each node. The displacement in the overlaid area was computed from the local and global meshes as follows as:

$$u(x)=\begin{cases}u^G(x) & x\in\Omega^G-\Omega^L\\ u^G(x)+u^L(x) & x\in\Omega^L\end{cases} \tag{1}$$

The strain at the overlaid area was computed by calculation summation of strain at the local and global area as follows:

$$\varepsilon(x)=\varepsilon^G(x)+\varepsilon^L(x) \tag{2}$$

The equation of principal of virtual work was related to the stress and strain relationship as follows:

$$\begin{aligned}&\int_\Omega\left\{\delta\varepsilon^G\right\}^T[D]\left\{\varepsilon^G\right\}d\Omega^{G-L}-\int_\Gamma\left\{\delta u^G\right\}^T\{f\}d\Gamma^{GL}\\&+\int_\Omega\left(\left\{\delta\varepsilon^G\right\}^T+\left\{\delta\varepsilon^L\right\}^T\right)[D]\left(\left\{\varepsilon^G\right\}+\left\{\varepsilon^L\right\}\right)d\Omega^L\\&-\int_\Gamma\left(\left\{\delta u^G\right\}^T+\left\{\delta u^L\right\}^T\right)\{f\}d\Gamma^L=0\end{aligned} \tag{3}$$

Where Ω^{G-L} represents the non-overlay area. In matrix form, the equation for S-FEM is:

$$\begin{bmatrix}K_{GG} & K_{GL}\\ K_{LG} & K_{LL}\end{bmatrix}\begin{Bmatrix}u^G\\ u^L\end{Bmatrix}=\begin{Bmatrix}F_G\\ F_L\end{Bmatrix} \tag{4}$$

where

$$[K_{GG}]=\int_{\Omega^G}\left[B^G\right]^T[D]\left[B^G\right]d\Omega^G$$

$$[K_{GL}]=\int_{\Omega^L}\left[B^G\right]^T[D]\left[B^L\right]d\Omega^L$$

$$[K_{LG}]=\int_{\Omega^L}\left[B^L\right]^T[D]\left[B^G\right]d\Omega^L$$

$$[K_{LL}]=\int_{\Omega^L}\left[B^L\right]^T[D]\left[B^L\right]d\Omega^L$$

The $[B]$ is the displacement-strain matrix and $[K]$ matrix is the stiffness matrix for local and global in the overlaid area. The nodal force, $\{F_L\}$ at the local area and the nodal force, $\{F_G\}$ at global area respectively. The displacement of each node is calculated by computing the equation 4 for both global and local meshes. The local mesh is changed the size and global mesh was not affected for it. The re-meshing process can be generated for a local area alone. The re-meshing process was needed for the fatigue crack growth model. Figure 2 shows the combination of local mesh with the global mesh. The combination was applied based on the boundary condition such as loading and constrain. In every iteration, the local mesh crack growth was expanded time by time until the fracture completed. The value of energy release rate is calculated for every new size of local mesh. The stress intensity factor (SIF) was obtained based from the calculation of energy release rate.

$$K_I = \sqrt{EG_I}, \quad K_{II} = \sqrt{EG_{II}}, \quad K_{III} = \sqrt{2\mu G_{III}} \tag{5}$$

E is Young's modulus of elasticity under the plane stress condition. For the plain strain condition the equation as follows $E/1\text{-}v^2$.The v is a Poisson's ratio. Fracture was analyzed by using the of linear fracture mechanics concepts; the crack propagation condition is assumed to be based upon the critical energy release rate. The energy release rate was utilized in the crack growth analysis.

The Virtual Crack Closure Method (VCCM) was applied in this analysis to determine the energy release rate [16]. The VCCM was examined the crack tip opening displacement that located near to the crack front. The VCCM were calculated by using the according to the equation:

$$G_{Total} = \frac{1}{2\Delta w^J} \sum_{I=1}^{5} C^I v_i^I P_i^I \tag{6}$$

where I is a nodes number that be located around the crack tip. The nodal force, P_i^I and the opening displacement, v_i^I at the five nodes at the front edge of the crack front. The triangle shape, Δ is the width of the element in the radial direction. The width of the element parallel is w^J to the crack front. The constant C^I is expressed as:

$$C^1 = C^2 = \frac{w^J}{w^{J+1} + w^J}, \quad C^3 = 1, \quad C^4 = C^5 = \frac{w^J}{w^{J-1} + w^J}, \tag{7}$$

The crack plane with a certain condition with VCCM implementation. The segments were used to define the displacement and stresses. The areas of the element before, S_2^J and after, S_1^J crack front are expressed as:

$$S_1^J = \int_{\theta_1}^{\theta_2}\int_0^{\Delta}(R+r)drd\theta = \int_{\theta_1}^{\theta_2}\left(\Delta R + \frac{\Delta^2}{2}\right)d\theta$$
$$S_2^J = \int_{\theta_1}^{\theta_2}\int_0^{\Delta}(R-\Delta+r)drd\theta = \int_{\theta_1}^{\theta_2}\left(\Delta R - \frac{\Delta^2}{2}\right)d\theta \quad (8)$$

The energy release rate, implemented by [16]. The equations are shown below:

$$G_I = \frac{K_I^2}{E} = \frac{1}{2\left[S_1^J - \frac{1}{4}\left(S_1^J - S_2^J\right)\right]}\int_{S_1^J}\sigma_{33}(r)v_3(\Delta - r)\,dS_1^J \quad (8)$$

$$G_{II} = \frac{1}{2\left[S_1^J - \frac{1}{4}\left(S_1^J - S_2^J\right)\right]}\int_{S_1^J}\sigma_{31}(r)v_1(\Delta - r)\,dS_1^J \quad (9)$$

$$G_{III} = \frac{1}{2\left[S_1^J - \frac{1}{4}\left(S_1^J - S_2^J\right)\right]}\int_{S_1^J}\sigma_{32}(r)v_2(\Delta - r)\,dS_1^J \quad (10)$$

$$G_{Total} = \frac{1}{2\left[S_1^J - \frac{1}{4}\left(S_1^J - S_2^J\right)\right]}\int_{S_1^J}\sigma_{3i}(r)v_i(\Delta - r)\,dS_1^J \quad (11)$$

where v_i is the crack opening displacement at the crack face and σ_{3i} is the cohesive stress at the local axis, x_3. Then, the energy release rate can be converted to the ΔK_{eq} via Eq.(5). The crack growth rate is expressed by Paris's law equation as follows:

$$\frac{dn}{dN} = C\left(\Delta K_{eq}\right)^n \quad (12)$$

Where N and da are the number of cycles and crack growth increment, respectively. C and n coefficients are material constants. The crack length is presented as:

$$da = C\left(\Delta K_{eq}\right)^n \times dN \quad (13)$$

The ΔK_{eq} is the equivalent SIF. It is a parameter that associated with the fatigue crack growth rate under mixed-mode conditions. The equivalent SIF ΔK_{eq} is presented by:

$$\Delta K_{eq} = \frac{\Delta K_I}{2} + \frac{1}{2}\sqrt{\Delta K_1^2 + 4\left(1.155\Delta K_{II}\right)^2 + 4\left(\Delta K_{III}\right)^2} \quad (14)$$

The crack growth angle, φ_o is influenced by the value of K_I, K_{II}, and K_{III}. Based on Richard et al. [17], the crack growth angle can be calculated as follows:

$$\varphi_o = \mp\left[140^\circ \frac{|K_{II}|}{K_I + |K_{II}| + |K_{III}|} - 70^\circ \left(\frac{|K_{II}|}{K_I + |K_{II}| + |K_{III}|}\right)^2\right] \quad (15)$$

where $\varphi_o < 0^\circ$ for $K_{II} > 0$ and $\varphi_o > 0^\circ$ for $K_{II} < 0$ and $K_I \geq 0$.

4. Results and discussion

Figure 4 is illustrated the beach marks for the surface crack growth of four-point bending and three-point bending model. Fracture surface is propagated when it reached a critical size. The models produce 6 beach marks based on their cycles of fatigue loading.

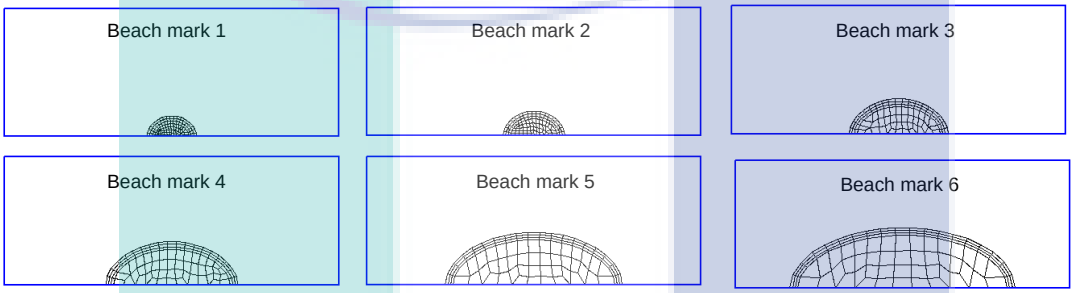

(a) Surface crack for four-point bending.

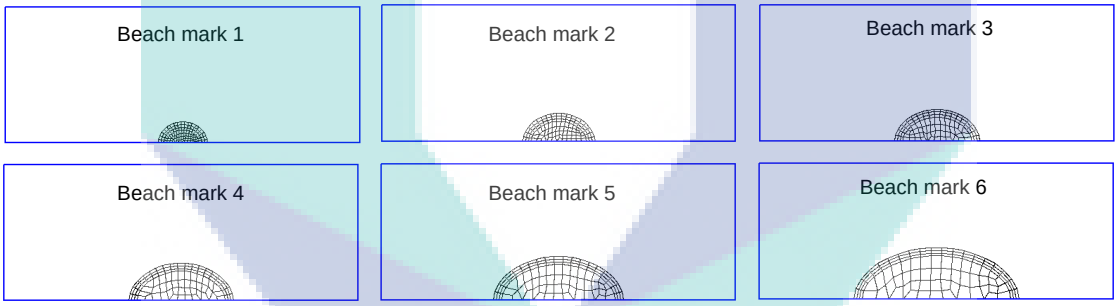

(b) Surface crack for three-point bending.

Figure 4. The beach marks surface fatigue crack.

Figure 5 shows the crack depth, *a* versus crack length, *c* based on the fatigue surface crack propagation. The surface crack from the four-point bending experiment produces five beach marks. The line of beach marks is presented in the graph by coordinate for a comparison. The crack is propagated from the initial flaws until completely fracturing. The S-FEM produces another beach marks to compare with experiment. Based on the obtained results, it was observed that the beach marks for experiment between S-FEM slightly different. The initial beach marks for S-FEM was same as the experiment and changed slightly until it fractures. The point of crack length for S-FEM was less than 20 percent differences between surface crack from the experiment. While the point of crack depth for S-FEM is moderately far apart from the experiment. In the overall graph, the S-FEM result is validated to compare with experiment result. The surface fatigue crack is computed by following Paris's law theory that stated in equation (14) and (15).

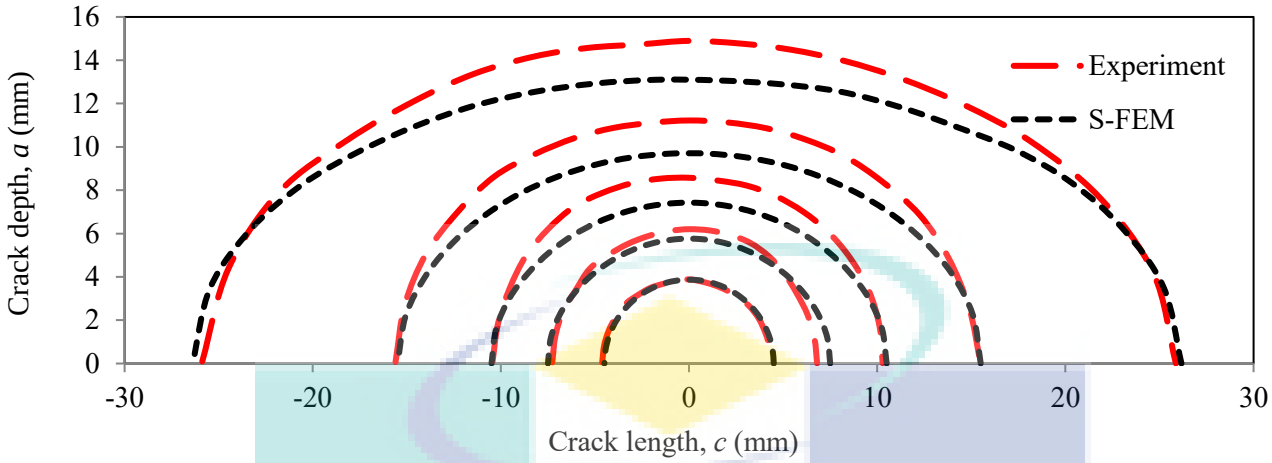

Figure 5. The comparison surface cracks four-point bending between Ohdama et al. [12] experiment.

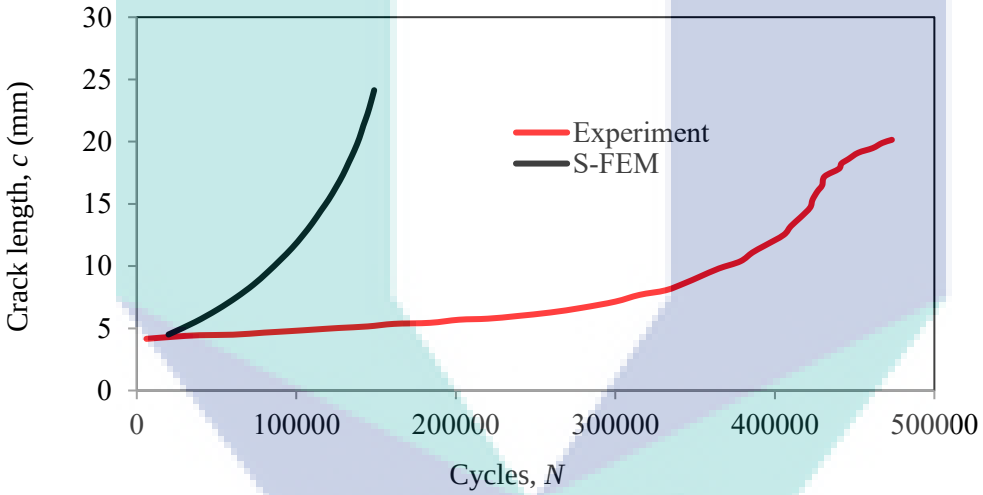

Figure 6. The fatigue life of four-point bending.

The crack length, c versus the cycles, N as a time period to crack growth rate until it a failure is shown in Figure 6. The fatigue life comparison from experiment between S-FEM is illustrated in Figure 6. The S-FEM is reached a maximum point at 20 mm crack length and 136382 cycles. While the experiment is reached a maximum point at 20 mm for crack length with 473367 cycles. There are significant difference of a maximum point between S-FEM and experiment. The S-FEM has quickly reached a failure compare with the experiment.

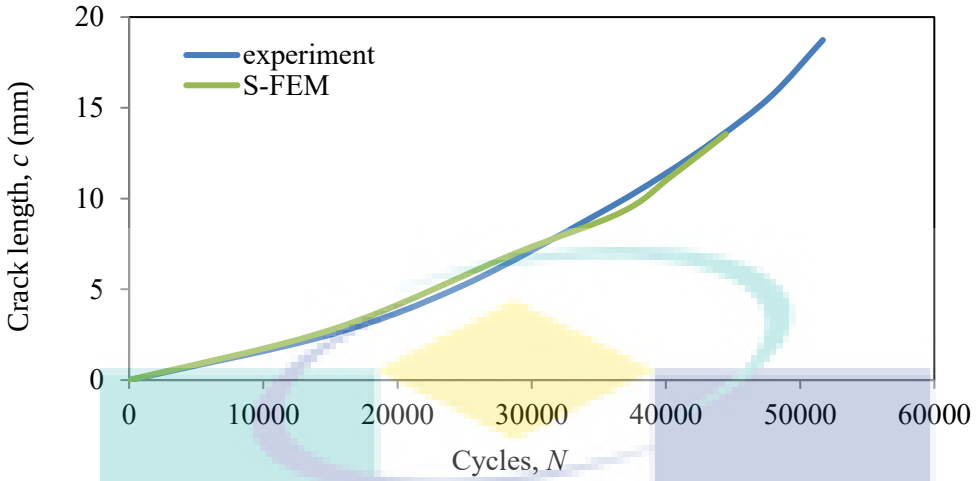

Figure 7. The fatigue life of Aluminium 2017-T3.

The experiment results from Kikuchi et al. [13] are presented to compare with S-FEM result for fatigue life of Aluminium 2017-T3 in three-point bending. Figure 7 is illustrated the fatigue life based on crack length, *c* versus cycles, *N* until it failure propagation. The S-FEM is achieved maximum point at 14 mm of crack length and 44463 N of cycles. Then, the experiment is reached a maximum point at 14 mm of crack length with 43856 N of cycles. The comparison of S-FEM and experiment is slightly accurate as a prediction.

5. Conclusions

The crack growth surface was simulated by S-FEM useful for prediction beach marks of a surface fatigue crack. The beach marks were produced from the S-FEM near with the experiment. Besides that, the fatigue life between four-point bending and three-point bending is produced a different result that compared with the experimental result. It was concluded the model of S-FEM for four-point bending had mistaken in meshing or error of coding S-FEM simulation. Further investigations of the numerical method in S-FEM are required to extend the present work.

Acknowledgments

The authors thankful to the Universiti Malaysia Pahang (UMP) and for financial support. This study was funded by RDU170383 from Universiti Malaysia Pahang (UMP) and Fundamental Research Grant Scheme (FRGS/1/2017/TK03/UMP/02/24) from Kementerian Pendidikan Malaysia (KPM) with number RDU170124.

References

1. Kamaludin, M.A., et al., *A fracture mechanics approach to characterising the environmental stress cracking behaviour of thermoplastics.* Theoretical and Applied Fracture Mechanics, 2017. **92**: p. 373-380.
2. Ma, C., et al., *An effective computational approach based on XFEM and a novel three-step detection algorithm for multiple complex flaw clusters.* Computers & Structures, 2017. **193**: p. 207-225.
3. Nilsson, K.F., N. Taylor, and P. Minnebo, *Analysis of fracture tests on large bend beams containing an embedded flaw.* International Journal of Pressure Vessels and Piping, 2006. **83**(1): p. 72-83.
4. Zhang, Y., Z. Xiao, and J. Luo, *Fatigue crack growth investigation on offshore pipelines with three-dimensional interacting cracks.* Geoscience Frontiers, 2017.

5. Feng, S.Z. and W. Li, *An accurate and efficient algorithm for the simulation of fatigue crack growth based on XFEM and combined approximations.* Applied Mathematical Modelling, 2018. **55**: p. 600-615.
6. O'Hara, P., C.A. Duarte, and T. Eason, *A two-scale generalized finite element method for interaction and coalescence of multiple crack surfaces.* Engineering Fracture Mechanics, 2016. **163**: p. 274-302.
7. Fish, J., *The s-version of the finite element method.* Computers & Structures, 1992. **43**(3): p. 539-547.
8. Düster, A. and E. Rank, *The p-version of the finite element method compared to an adaptive h-version for the deformation theory of plasticity.* Computer Methods in Applied Mechanics and Engineering, 2001. **190**(15): p. 1925-1935.
9. Babuška, I. and M. Suri, *The p- and h-p versions of the finite element method, an overview.* Computer Methods in Applied Mechanics and Engineering, 1990. **80**(1): p. 5-26.
10. Schmidt, A. and K.G. Siebert, *A posteriori estimators for the h – p version of the finite element method in 1D.* Applied Numerical Mathematics, 2000. **35**(1): p. 43-66.
11. Kikuchi, M., Y. Wada, and K. Suga, *Surface crack growth simulation under mixed mode cyclic loading condition.* Procedia Engineering, 2011. **10**: p. 427-432.
12. Ohdama, C., *Effect Of KIII On Fatigue Crack Growth Behavior*, in *Department of Mechanical Engineering*. 2012, Tokyo University of Science, Japan [in Japanese]: Yamazaki, Chiba.
13. Masanori Kikuchi, Y.W., Maigefeireti Maitireyimu and Hirotaka Sano *Closure Effect on Interaction of Two Surface Cracks Under Cyclic Bending.* ASME 2010 Pressure Vessels and Piping Conference, 2010. **Volume 1**.
14. McFadyen, N.B., R. Bell, and O. Vosikovsky, *Fatigue crack growth of semi-elliptical surface cracks.* International Journal of Fatigue, 1990. **12**(1): p. 43-50.
15. Shi, K., et al., *A theoretical model of semi-elliptic surface crack growth.* Chinese Journal of Aeronautics, 2014. **27**(3): p. 730-734.
16. Okada, H., et al., *Three dimensional virtual crack closure-integral method (VCCM) with skewed and non-symmetric mesh arrangement at the crack front.* Engineering Fracture Mechanics, 2005. **72**(11): p. 1717-1737.
17. Richard, H.A., M. Fulland, and M. Sander, *Theoretical crack path prediction.* Fatigue & Fracture of Engineering Materials & Structures, 2005. **28**(1-2): p. 3-12.

Kesimpulan

Overall, the ProbS-FEM was developed to consider the uncertainties in the analysis. The verification of the developed code was presented to show the capability of the ProbS-FEM in predicting the SIF, the crack growth for different modes of loading, and the fatigue life distribution. Single and multiple surface cracks were simulated to indicate the level of complexity that could be solved by the ProbS-FEM. The new understanding of the SIF, crack growth and fatigue life distribution, particularly for the case of single and multiple surface cracks, have been discussed. The integrity of the components could be observed through the ProbS-FEM analysis. The ProbS-FEM produced a range of outputs because of the existence of uncertainty in the material properties and the crack initiation. The new contribution has improved the previous solution model that mostly revealed the static or deterministic results only. The range of outputs produced in the ProbS-FEM provided a remedy for stray deterministic predictions, particularly in fatigue behaviour. Computationally, the application of the probabilistic approach by the developed algorithm contributed to the enhancement of the S-FEM compared to the previous approach.

The work that has been carried out provides several promising avenues for further probabilistic surface crack researches as follows:
(i) The dispersion of the presented initial surface crack size was limited to the standard deviation approach. Thus, a study on a new methodology to calculate the equivalent initial flaw size distribution is highly encouraged. The initial flaw size distribution should be determined to confirm the changes in the fatigue life results.
(ii) The variable amplitude loading for mode *I* and *II* with the same geometrical model should be conducted to assess the change in the mixed mode fracture, and the dominant mode can be determined. In addition, it is essential to consider the introduction of a variable amplitude load in the ProbS-FEM. The variable amplitude load exposes the scatter input in an analysis.

Rujukan

Aguilarespinosa, A. A., Fellows, N. A. & Durodola, J. F. 2013. Experimental Measurement of Crack Opening and Closure Loads for 6082-T6 Aluminium Subjected to Periodic Single and Block Overloads and Underloads. International Journal of Fatigue 47: 71-82.

Akramin, M. R. M. 2008. Analisis Kegagalan Struktur Retak Menggunakan Kaedah Hibrid Unsur Terhingga Dan Monte Carlo. Master Thesis, Department of Mechanical & Materials Engineering, Universiti Kebangsaan Malaysia [in Malaysian].

Anderson, T. L. 2005. Fracture Mechanics: Fundamentals and Applications. 3rd. Boca Raton: Taylor & Francis Group,CRC.

Angioni, S. L., Visrolia, A. & Meo, M. 2012. Combining X-Fem and a Multilevel Mesh Superposition Method for the Analysis of Thick Composite Structures. Composites Part B: Engineering 43: 559-568.

ASTM E740-03. 2008. Standard Practice for Fracture Testing with Surface-Crack Tension Specimens, Section 3. West Conshohocken, USA.

Barker, V. M., Steven Johnson, W., Adair, B. S., Antolovich, S. D. & Staroselsky, A. 2013. Load and Temperature Interaction Modeling of Fatigue Crack Growth in a Ni-Base Superalloy. International Journal of Fatigue 52: 95-105.

Beden, S. M. 2010. Assessment of Fatigue Crack Growth under Variable Amplitude Loading. PhD Thesis, Mechanical and Materials Department, Faculty of Engineering and Built Environment, Universiti Kebangsaan Malaysia.

Beden, S. M., Abdullah, S. & Ariffin, A. K. 2009. Review of Fatigue Crack Propagation Models for Metallic Components. In. (edit.). European Journal of Scientific Research, 28. pp. 364-397. EuroJournals Publishing, Inc.

Beer, M. & Liebscher, M. 2008. Designing Robust Structures – a Nonlinear Simulation Based Approach. Computers & Structures 86: 1102-1122.

Berer, M. & Pinter, G. 2013. Determination of Crack Growth Kinetics in Non-Reinforced Semi-Crystalline Thermoplastics Using the Linear Elastic Fracture Mechanics (Lefm) Approach. Polymer Testing 32: 870-879.

Brighenti, R. 2001. External Longitudinal Flaws in Pipes under Complex Loading. Journal of Pressure Vessel Technology, Transactions of the ASME 123: 139-145.

Brighenti, R. & Carpinteri, A. 2013. Surface Cracks in Fatigued Structural Components: A Review. Fatigue and Fracture of Engineering Materials and Structures 36: 1209-1222.

Broek, D. 1986. Elementary Engineering Fracture Mechanics. AD Dordrecht, The Netherlands: Kluwer Academic Publishers.

Cai, T., Wang, S. & Xu, Q. 2015. Monte Carlo Optimization for Site Selection of New Chemical Plants. Journal of Environmental Management 163: 28-38.

Cai, Y., Han, L., Tian, L. & Zhang, L. 2016. Meshless Method Based on Shepard Function and Partition of Unity for Two-Dimensional Crack Problems. Engineering Analysis with Boundary Elements 65: 126-135.

Carpinteri, A. 1993. Shape Change of Surface Cracks in Round Bars under Cyclic Axial Loading. International Journal of Fatigue 15: 21-26.

Carpinteri, A., Brighenti, R. & Vantadori, S. 2009. Notched Double-Curvature Shells with Cracks under Pulsating Internal Pressure. International Journal of Pressure Vessels and Piping 86: 443-453.

Carpinteri, A., Ronchei, C. & Vantadori, S. 2013. Stress Intensity Factors and Fatigue Growth of Surface Cracks in Notched Shells and Round Bars: Two Decades of Research Work. Fatigue and Fracture of Engineering Materials and Structures 36: 1164-1177.

Carpinteri, A. & Vantadori, S. 2009. Sickle-Shaped Cracks in Metallic Round Bars under Cyclic Eccentric Axial Loading. International Journal of Fatigue 31: 759-765.

Carpinteri, A. & Vantadori, S. 2009. Sickle-Shaped Surface Crack in a Notched Round Bar under Cyclic Tension and Bending. Fatigue and Fracture of Engineering Materials and Structures 32: 223-232.

Cendõn, D. A., Torabi, A. R. & Elices, M. 2015. Fracture Assessment of Graphite V-Notched and U-Notched Specimens by Using the Cohesive Crack Model. Fatigue and Fracture of Engineering Materials and Structures 38: 563-573.

Cetin, A., Härkegård, G. & Naess, A. 2013. The Fatigue Limit: An Analytical Solution to a Monte Carlo Problem. International Journal of Fatigue 55: 194-201.

Choi, S., Grandhi, R. V. & Canfield, R. A. 2007. Reliability-Based Structural Design. 1st. London: Springer.

Chowdhury, M. S., Song, C. & Gao, W. 2014. Probabilistic Fracture Mechanics with Uncertainty in Crack Size and Orientation Using the Scaled Boundary Finite Element Method. Computers & Structures 137: 93-103.

Daud, R. 2012. Analysis of Elastic Interacting Cracks in Finite Body. PhD Thesis, Department of Mechanical & Materials Engineering, Universiti Kebangsaan Malaysia.

De Matos, P. F. P. & Nowell, D. 2009. Experimental and Numerical Investigation of Thickness Effects in Plasticity-Induced Fatigue Crack Closure. International Journal of Fatigue 31: 1795-1804.

Dong, Y., He, X., Xue, D. & Liu, W. 2015. Sif Solution for a Single Hole-Edge Crack in a Finite Plate with Clamped Ends. Yingyong Lixue Xuebao/Chinese Journal of Applied Mechanics 32: 187-191.

Doshi, K. & Vhanmane, S. 2013. Probabilistic Fracture Mechanics Based Fatigue Evaluation of Ship Structural Details. Ocean Engineering 61: 26-38.

Dowling, N. E. 1999. Mechanical Behavior of Materials. 2nd Edition. Prentice Hall.

Dugdale, D. S. 1960. Yielding of Steel Sheets Containing Slits. J. Mech. Phys. Solids 8: 100.

Duquesnay, D. L. & Underhill, P. R. 2010. Fatigue Life Scatter in 7xxx Series Aluminum Alloys. International Journal of Fatigue 32: 398-402.

El-Zeghayar, M., Topper, T. H., Conle, F. A. & Bonnen, J. J. F. 2011. Modeling Crack Closure and Damage in Variable Amplitude Fatigue Using Smooth Specimen Fatigue Test Data. International Journal of Fatigue 33: 223-231.

Elishakoff, I. & Ren, Y. 1999. The Bird's Eye View on Finite Element Method for Structures with Large Stochastic Variations. Computer Methods in Applied Mechanics and Engineering 168: 51-61.

Emery, J. M., Hochhalter, J. D., Wawrzynek, P. A., Heber, G. & Ingraffea, A. R. 2009. Ddsim: A Hierarchical, Probabilistic, Multiscale Damage and Durability Simulation System – Part I: Methodology and Level I. Engineering Fracture Mechanics 76: 1500-1530.

Estecahandy, M., Bordes, L., Collas, S. & Paroissin, C. 2015. Some Acceleration Methods for Monte Carlo Simulation of Rare Events. Reliability Engineering & System Safety 144: 296-310.

Feng, Z., Mao, K., Zou, T. & Yang, Y. 2014. Discussion on Airworthiness Requirement of Widespread Fatigue Damage – Safe-Life Methodology or Damage-Tolerance Methodology. Procedia Engineering 80: 392-398.

Fish, J. 1992. The S-Version of the Finite Element Method. Computers & Structures 43: 539-547.

Forth, S. C., Everett, R. A. & Newman, J. A. 2002. A Novel Approach to Rotorcraft Damage Tolerance. 6th joint FAA/DoD/NASA aging aircraft conference, pp. 1-18.

Lampiran

None